Wireless-Powered Distributed Spatial Modulation with Energy Recycling and Finite Energy Storage

Sandeep Narayanan, *Member, IEEE*, Mohammad Shikh-Bahaei, *Senior Member, IEEE*, Jiancao Hou, *Member, IEEE*, and Mark F. Flanagan, *Senior Member, IEEE*

***Abstract*—The Distributed Spatial Modulation (DSM) protocol, which allows relays to forward the source's data while simultaneously allowing the relays to transmit their own data, has been proposed in [1]. In this paper, we introduce two new protocols for enabling DSM, consisting of single-antenna network nodes, with simultaneous wireless information and power transfer (SWIPT) capability: Power splitting based DSM (PS-DSM) and energy recycling based DSM (ER-DSM). More specifically, PS-DSM relies on power splitters at the relay nodes to harvest energy transmitted from the source. On the other hand, ER-DSM, by exploiting the inactive cooperating relays in DSM-based protocols, recycles part of the transmitted energy in the network, without relying on power splitters or time switches at the relays to harvest energy. This leads to an increase in the average harvested energy at the relays with reduced hardware complexity. Both PS-DSM and ER-DSM also retain all the original features of DSM. Due to its particular operating principle and specific advantages, we select ER-DSM as the candidate for further mathematical analysis. More specifically, by considering a multi-state battery model, we propose an analytical framework based on a Markov chain formulation for modelling the charging/discharging behaviour of the batteries at the relay nodes in ER-DSM. Furthermore, based on the derived Markov chain model, we introduce a mathematical framework for computing the error probability of ER-DSM, by explicitly taking into account the effect of finite-sized batteries. The frameworks are substantiated with the aid of Monte Carlo simulations for various system setups.**

***Index Terms*—Spatial Modulation, SWIPT, Relaying, Markov chain, Performance Analysis.**

I. Introduction

One of the emerging paradigms in the field of green wireless communications is that of so-called "energy-neutral" networks. In these networks, the network elements harvest energy from various sources, such as solar, wind, motion, etc., or from other Radio Frequency (RF) sources, and use the harvested energy for transceiver operations. The RF energy harvesting technology, in particular, is a more suitable candidate for applications where Quality-of-Service (QoS) is of paramount importance. The simultaneous wireless information and power transfer (SWIPT) is an RF energy harvesting technology where other nodes in the network can concurrently convey wireless information and energy to an energy-deficient mobile node [2], [3]. Therefore, SWIPT has the capability to provide higher spectral efficiencies compared to other RF energy harvesting technologies. Furthermore, the advent of ultra-dense heterogeneous networks, device-device networks [4], and large-scale multiple-antenna systems (LSMAS) also complements the integration of SWIPT technology to 5G and beyond-5G networks. Another emerging trend that supports the SWIPT technology is cellular-enabled IoT, which connects potentially billions of low-energy devices. Using the SWIPT technology, these low-energy devices can transmit information via their cellular connection, as well as recharge their battery.

In general, SWIPT can be realized in practice using three main techniques [3], [5]: 1) *power splitting* (PS), where the receiver splits the received signal into two parts – one part for information decoding, and the other for energy harvesting; 2) *time switching* (TS), where the receiver alternatively switches between information decoding and energy harvesting for specific time durations; and 3) *antenna switching* (AS), where the multiple antennas at the receiver are allocated appropriately to information decoding and to energy harvesting. It is well-understood that power splitters and time switches increase, by a considerable margin, the hardware complexity and cost of the energy harvesting device. On the other hand, AS does not require dedicated hardware components, and is therefore a more practical as well as a low-complexity solution to implement SWIPT. Recently, SWIPT has been investigated in the context of Multiple-Input-Multiple-Output (MIMO) networks, *e.g.*, [5]–[7], and in the context of cooperative relay-aided networks, *e.g.*, [8]–[17], with/without the consideration of energy harvesting units, *e.g.*, rechargeable batteries. A comprehensive survey is available in [18], to which the interested reader is referred for further information.

Spatial Modulation (SM), a single-RF MIMO scheme, has become a potential air-interface transmission technology for 5G cellular networks [19], [20]. In general, SM encodes the incoming bit-stream onto the Channel State Information (CSI) of one of the active antennas (*i.e.*, spatial domain) as well as onto the complex modulated symbol transmitted from this active antenna (*i.e.*, signal domain). Since only one antenna

Manuscript received July 24, 2017; revised December 18, 2017; and May 14, 2018, accepted July 13, 2018. This work was supported in part by the Science Foundation Ireland through the project CooperaNET (Grant 13/CDA/2199), and in part by the Engineering and Physical Sciences Research Council through the project SENSE (Grant EP/P003486/1). The associate editor coordinating the review of this paper and approving it for publication was Dr. Christopher Anderson

S. Narayanan was with the School of Electrical and Electronic Engineering, University College Dublin, Belfield, Dublin 4, Ireland. He was also with the Centre for Telecommunications Research, Department of Informatics, King's College London, London WC2R 2LS, U.K. (e-mail: sandeep.kadanveedu@kcl.ac.uk).

M. Shikh-Bahaei and J. Hou are with the Centre for Telecommunications Research, Department of Informatics, King's College London, London WC2R 2LS, U.K. (jiancao.hou@kcl.ac.uk; m.sbahaei@kcl.ac.uk).

M. F. Flanagan is with University College Dublin, School of Electrical and Electronic Engineering, Belfield, Dublin 4, Ireland (e-mail: mark.flanagan@ucd.ie).

needs to be active, and two information-carrying units are used to convey information, SM, when combined with LSMAS, has the potential to satisfy future demands of mobile data traffic. More importantly, these data demands can be satisfied with low implementation and computational complexity compared to traditional MIMO-based LSMAS systems [21]–[24]. More recently, in addition to the spatial and signal domains, the polarisation domain of the antennas has also been exploited to further improve the spectral efficiency of SM [25]. Several authors have also investigated the application of SM to relay-aided networks, *e.g.*, [1], [26]–[29], LSMAS/massive MIMO systems, *e.g.*, [30], [31], full-duplex wireless systems, *e.g.*, [32], [33], millimeter wave communications, *e.g.*, [34], [35], and SWIPT-enabled systems, *e.g.*, [36], [37]. A comprehensive survey of SM is available in [38].

In particular, the application of SM to SWIPT-enabled wireless systems is relatively new; however, this has been receiving considerable attention recently. The main reason for this interest is that SM has the potential to leverage the (multiple) inactive antennas for harvesting energy without compromising on the achievable information rate. More specifically, in [36], a PS-based SWIPT is considered for an SM system with co-located antennas at the transmitter and the receiver. The authors develop an iterative algorithm to maximize the information throughput under certain energy harvesting constraints. In [37], a multi-antenna wireless device employing SM is considered to be harvesting energy transmitted from an energy transmitter, with the aid of AS, while simultaneously communicating to an information receiver. As promising as they are, however, neither of these works has considered the availability of an energy storage device at the harvesting node. Indeed, the storage device enables energy accumulation at the harvesting node and therefore, leads to a more effective solution to use the harvested energy. Against this background, in this paper we consider SWIPT in the context of distributed SM (DSM) [1], which enables the implementation of SM using single-antenna mobile terminals. Before going into the details, however, we first briefly review the concept of DSM in what follows.

A. Brief Review of DSM

The concept of DSM was proposed in [29], and was studied more extensively in [1]. The distinguishable feature of DSM lies in allowing the single-antenna network nodes to act as relays to forward the data of the source, while simultaneously allowing the relays to transmit their own data. The basic idea is to encode the source's data onto the spatial position of the cooperating relays, and exploit the signal domain to transmit the data of the relays. In more detail, each of the relay nodes is assigned a unique identifier or a digital signature which is in the form of unique bit-sequence. The data symbol received from the source is used as the "activation symbol", *i.e.*, whenever there is a match between the random bit-sequence transmitted by the source and the relay's own identifier, that particular relay is activated, and the remaining relays are kept silent. Once activated, the relay will only transmit its own data. The destination, on the other hand, will jointly decode the data transmitted by both the source and the relays by exploiting the distinct channel impulse responses associated with the spatial position of the active relays. Consequently, the average aggregate throughput of DSM is considerably higher compared to that of conventional relay networks, where the relays have to incur delay, as well as spend their own energy to forward the source's data. Furthermore, it is also shown in [1] that DSM is capable of outperforming several closely related state-of-the-art relaying protocols, including superposition modulation [40]. It is worth emphasizing here that in DSM, *only a single cooperating relay is required to be active at any time instance* (if there are no demodulation errors at the relays). Furthermore, the activation decision is taken independently by each relay and without any coordination among them. Therefore, the symbol-level inter-relay synchronization requirements are less stringent, as simultaneous relay transmissions are not required. If there are potential demodulation demodulation errors at the relays, however, since multiple relays may be active simultaneously, our protocol necessitates symbol-level synchronization among the relays, similar to traditional distributed multi-relay protocols.

B. Paper Contribution

Having summarized the main advantages of the DSM protocol [1], in the present paper we are aim to propose protocols for wireless-powered DSM. In particular, the novelty and contribution of the present paper are as follows:

- We introduce two new protocols for enabling DSM, consisting of single-antenna network nodes, with SWIPT capability: PS-based DSM (PS-DSM) and energy recycling based DSM (ER-DSM). More specifically, PS-DSM relies on power splitters at the relay nodes to harvest energy transmitted from the source. On the other hand, ER-DSM, by exploiting the inactive cooperating relays in DSM-based protocols, recycles part of the transmitted energy in the network, without relying on power splitters or time switches at the relays to harvest energy. This leads to an increase in the average harvested energy at the relays with reduced hardware complexity. Both PS-DSM and ER-DSM also retain the original features of DSM, including the property that allows relays to forward the source's data while simultaneously transmitting their own data.
- Due to its particular operating principle and specific advantages, we select ER-DSM as the candidate for further mathematical analysis. The proposed ER-DSM protocol finds its inspiration from the work on self-energy recycling in [13]. In [13], however, an amplify-and-forward relay network with a single multi-antenna relay is considered, and the authors optimize the system throughput under certain energy harvesting constraints. Furthermore, the possible integration of a rechargeable battery at the relay node has not been taken into account. The mathematical analysis of PS-DSM is not considered in the present paper due to space limitations. However, an analytical development similar to that proposed for ER-DSM may be applied. Our specific contributions with regards to ER-DSM are summarized in what follows.

- By considering a multi-state battery model, we propose an analytical framework based on a Markov chain formulation for modelling the charging/discharging behaviour of the batteries at the relay nodes in ER-DSM.
- Based on the above Markov chain model, we introduce an accurate mathematical framework for computing the *error probability* of ER-DSM, by explicitly taking into account the effect of finite-sized batteries.
- The mathematical frameworks are substantiated with the aid of Monte Carlo simulations. Furthermore, it is also shown that ER-DSM is capable of outperforming PS-DSM for certain system setups [39].

C. Paper Organization

The remainder of the present paper is organized as follows. In Section II, the system models for PS-DSM and ER-DSM are described. In addition, the battery modeling assumptions are introduced. In Section III, the PS-DSM protocol is introduced and the corresponding demodulator is provided. In Section IV, the ER-DSM protocol is introduced. In Section V, the Markov chain analysis for modelling the behaviour of the relay batteries in ER-DSM is provided. In Section, VI, a mathematical framework for computing the error probability of ER-DSM is proposed. In Section VII, numerical results to substantiate the analytical findings and to compare ER-DSM against PS-DSM and the SWIPT-aided DemF protocol are shown. Finally, Section VIII concludes this paper.

D. Notation

$\Pr\{\cdot\}$ denotes probability. $\Pr\{A|B\}$ denotes the conditional probability of A under a given condition B. $(\cdot)^*$ and $|\cdot|$ denote complex conjugate and absolute value operators, respectively. $\mathbb{E}_X\{\cdot\}$ denotes the expectation computed with respect to the Random Variable (RV) X. $F_X(\cdot)$ denotes the Cumulative Distribution Function (CDF) of the RV X. $\mathrm{Re}\{\cdot\}$ and $\mathrm{Im}\{\cdot\}$ denote real and imaginary part operators. $j=\sqrt{-1}$ denotes the imaginary unit. $Q(x)=\left(1/\sqrt{2\pi}\right)\int_x^{+\infty}\exp\left(-t^2/2\right)dt$ denotes the Q-function. $\mathrm{card}\{\cdot\}$ denotes the cardinality of a set. Bold symbols denote strings of bits with fixed length. The function $(x)^+$ is defined as $(x)^+=x$ if $x\geq 0$, and $(x)^+=0$ if $x<0$. The function $\mathbb{1}_X(x)$ is the indicator function, *i.e.*, $\mathbb{1}_X(x)=1$ if $x\in X$ and $\mathbb{1}_X(x)=0$ if $x\notin X$. The function $\delta(a,b)$ is defined as $\delta(a,b)=1$ if $a\neq b$ and $\delta(a,b)=0$ if $a=b$, and we denote $\overline{\delta}(a,b)=1-\delta(a,b)$. The function $\rho(a,b)$ is defined as $\rho(a,b)=1$ if $a<b$ and $\rho(a,b)=0$ if $a\geq b$. Finally, we define $\overline{\rho}(a,b)=1-\rho(a,b)$.

II. Wireless-Powered DSM: System Model

We consider a network topology with one source (S), M half-duplex relays (R_r, where $r=1,2,...,M$) and one destination (D). All the nodes are equipped with a single antenna, which at any given time instance can be used either for transmission or for information decoding/energy harvesting. Both the source and the relays have *independent* data that need to be transmitted to the destination. The source and the relays (when active) transmit a complex modulated symbol with constellation sizes M and N, respectively. These symbols can be chosen from a Phase Shift Keying (PSK) or Quadrature Amplitude Modulation (QAM) constellation. The signal constellation used at the source is denoted as χ_S, and the signal constellation used at the relays is denoted as χ_R. Similar to DSM, in wireless-powered DSM, each relay is assigned a unique digital identifier $\mathbf{ID}_{R_r}$ for $r=1,2,\ldots,M$, which is a string of $\log_2(M)$ bits. Without loss of generality, a lexicographic labeling is used throughout this paper. If $M=4$, for example, the four relays are uniquely identified by the bit strings $\mathbf{ID}_{R_1}=00$, $\mathbf{ID}_{R_2}=01$, $\mathbf{ID}_{R_3}=10$ and $\mathbf{ID}_{R_4}=11$. We assume that a direct link is not available between the source and the destination, and that the source can communicate with the destination only with the aid of the relays.

Each cooperation phase in wireless-powered DSM lasts two time slots and consists of two sub-phases (more details are provided in the sequel), each of equal duration. For ease of notation, time indices are only provided where relevant. We assume quasi-static fading channels, where the channels remain static over one cooperative phase and change independently from one phase to another. According to the Friis propagation model [42]–[43], the fading coefficient between two generic network nodes X and Y is denoted as $h'_{XY}=h_{XY}/\sqrt{L_{XY}}$, where h_{XY} is a circularly symmetric complex Gaussian random variable with mean zero and variance $1/2$ per dimension, and $L_{XY}=\left(\frac{4\pi\mathcal{D}_{XY}f_{carr}}{c}\right)^2\frac{1}{G_XG_Y}$ is the free-space path-loss, with $\mathcal{D}_{XY}$ being the distance between node X and node Y, f_{carr} being the carrier frequency, G_X and G_Y denote the directional gains of the transmit antenna at node X and the receive antenna at node Y, respectively, and $c=3\times10^8$ m/s is the speed of light. Furthermore, fading over different wireless links are assumed to be independent non-identically distributed (i.n.i.d). The term $n_{XY}^{(\mathrm{a})}$ denotes the baseband Additive White Gaussian Noise (AWGN) introduced by the receiver antenna at node Y and related to the transmission from X. Similarly, $n_{XY}^{(\mathrm{c})}$ denotes the AWGN introduced during the conversion of the received signal from radio frequency to baseband [8]. Both $n_{XY}^{(\mathrm{a})}$ and $n_{XY}^{(\mathrm{c})}$ are complex Gaussian RVs with zero mean and variance per dimension $N_{\mathrm{A}}/2$ and $N_{\mathrm{C}}/2$, respectively. Furthermore, $n_{XY}^{(\mathrm{a})}$ and $n_{XY}^{(\mathrm{c})}$ at different time slots or at the input of different nodes are assumed to be independent and identically distributed (i.i.d.). For simplicity, we also introduce the notation $N_0=N_{\mathrm{A}}+N_{\mathrm{C}}$.

Each relay, R_r for $r=1,2,...,M$, is equipped with a single energy battery. In this paper, we adopt the widely used discrete-level model for the relay batteries [15]–[17]. All the relay batteries are considered to be of finite size, $E_{\max}=\kappa_R E_S$, with $\kappa_R>0$ being the battery scaling factor and E_S being the source's average transmit energy per symbol. The number of discrete energy levels at each battery is $L+2$. The i-th energy level of the battery at each relay is given as $\mathcal{E}^{(i)}=iE_{\max}/(L+1)$, for $i=0,1,...,L+1$. Here, $\mathcal{E}^{(0)}$ represents the empty level, and $\mathcal{E}^{(L+1)}$ represents the maximum possible level. When L is sufficiently large, the adopted discrete model of the relay batteries can be tightly

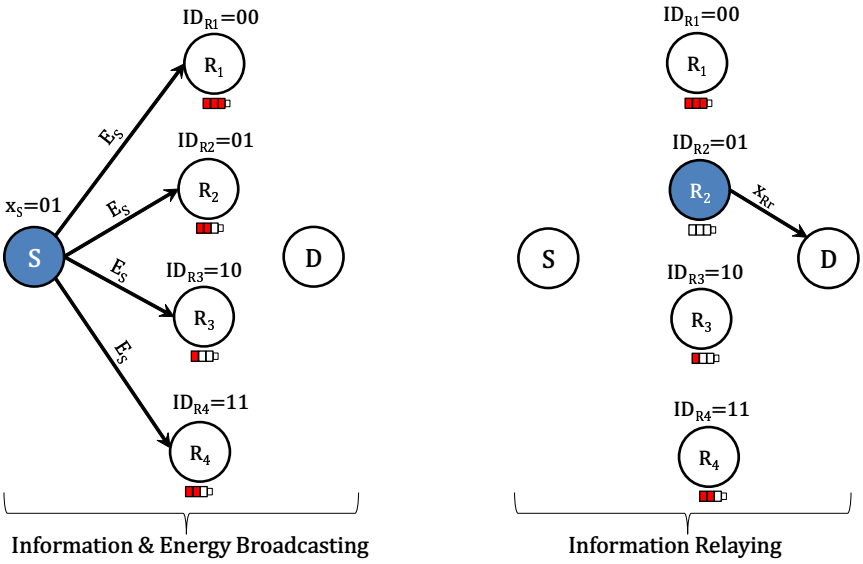

Fig. 1: Illustration of PS-DSM protocol for $M = 4$.

approximated to a continuous linear battery model [15]. In what follows, we describe in detail the proposed PS-DSM and ER-DSM protocols.

III. Power Splitting Based DSM

The PS-DSM protocol is illustrated in Fig. 1. In PS-DSM, we consider that each relay is equipped with power splitting circuitry which splits the received signal in two parts - one part for information decoding, and the other for energy harvesting. PS-DSM consists of two transmission phases: The first is the simultaneous information and energy broadcasting phase, and the second is the information relaying phase. Both transmission phases are described in what follows.

A. Simultaneous Information & Energy Broadcasting Phase

In this phase, the source broadcasts, with energy E_S, its data x_S to the M distributed relays. The power splitter at each relay R_r for $r = 1, 2, ..., M$, splits the received energy of the signal such that $\alpha_{R_r}^{(\mathrm{PS})}$, with $0 < \alpha_{R_r}^{(\mathrm{PS})} < 1$, portion of the received signal energy goes to its *energy receiver*, and the remaining $\left(1 - \alpha_{R_r}^{(\mathrm{PS})}\right)$ portion is directed to its *information receiver*. The interested reader is referred to [41] for further information on power splitting circuitry. Accordingly, the signal received at the information receiver of the relays can be formulated as follows ($r = 1, 2, ..., M$):

$$y_{SR_r} = \sqrt{\left(1 - \alpha_{R_r}^{(\mathrm{PS})}\right) E_S} h'_{SR_r} \mathcal{M}_S\left(\mathbf{x}_S\right) + \sqrt{\left(1 - \alpha_{R_r}^{(\mathrm{PS})}\right)} n_{SR_r}^{(\mathrm{a})} + n_{SR_r}^{(\mathrm{c})} \tag{1}$$

where $\mathcal{M}_S\left(\mathbf{x}_S\right) \in \chi_S$ is the complex modulated symbol transmitted by the source, with $\mathbf{x}_S$ being the $\log_2\left(M\right)$ bits for transmission by the source, and $\mathcal{M}_S\left(\cdot\right)$ is the bit-to-symbol modulation mapping function at the source.

Each relay independently demodulates the signal received from the source using the maximum-likelihood (ML) criterion as shown in (2), where $\widehat{\mathbf{x}}_S^{(R_r)}$ is the source's estimated bits at the relay R_r and $\widetilde{\mathbf{x}}_S^{(R_r)}$ represents the trial bits used in the hypothesis-detection problem at R_r.

The portion of the energy that is sent to the energy receiver at the relay R_r is $\alpha_{R_r}^{(\mathrm{PS})} E_S$. Therefore, based on the discrete-level model of the relay batteries given in Section II, the energy remaining at R_r after harvesting can be formulated as follows ($r = 1, 2, ..., M$) [15] as shown in (3), where $\eta \in (0, 1]$ denotes the energy conversion efficiency, and $\widetilde{\mathcal{E}}_{R_r}$ is the residual energy in the battery of relay R_r immediately prior to the energy harvesting process. Note that for the next information and energy broadcasting phase of PS-DSM,

$$\widehat{\mathbf{x}}_S^{(R_r)} = \underset{\mathcal{M}_S\left(\widetilde{\mathbf{x}}_S^{(R_r)}\right) \in \chi_S}{\arg\min} \left\{ \left| y_{SR_r} - \sqrt{\left(1 - \alpha_{R_r}^{(\mathrm{PS})}\right) E_S} h'_{SR_r} \mathcal{M}_S\left(\widetilde{\mathbf{x}}_S^{(R_r)}\right) \right| \right\} \tag{2}$$

$$\mathcal{E}_{R_r} = \max_{i \in \{0,1,...,L+1\}} \left\{ \mathcal{E}^{(i)} : \mathcal{E}^{(i)} < \widetilde{\mathcal{E}}_{R_r} + \eta \left(\alpha_{R_r}^{(\mathrm{PS})} E_S |h'_{SR_r}|^2 |\mathcal{M}_S\left(\mathbf{x}_S\right)|^2 \right) \right\} \tag{3}$$

$\widetilde{\mathcal{E}}_{R_r} = \mathcal{E}_{R_r}$ if R_r was inactive[1] during the information relaying phase. On the other hand, if R_r was active, we would have $\widetilde{\mathcal{E}}_{R_r} = (\mathcal{E}_{R_r} - E_{R_r})^+$, where E_{R_r} is the relay's transmit energy.

B. Information Relaying Phase

In this phase, the M distributed relays apply the SM principle in a distributed fashion to simultaneously forward the source's estimated data and the relay's *own* data. More specifically, the source's demodulated bit sequence at relay R_r, available from (2), is compared against its own unique ID. If there is match, that particular relay is activated for transmission, otherwise, it remains silent. When active, the relay transmits its own data using QAM/PSK modulation. In other words, the source's data is forwarded *implicitly* using the relay activation process, and the (active) relay's own data is transmitted *explicitly* from the relay using a complex modulated symbol. Accordingly, the signal received at the destination during this phase can be formulated as follows[2]:

$$y_{RD} = \sum_{r \in \Omega_R^{(\mathrm{ON})}} \sqrt{E_{R_r}} h'_{R_r D} \mathcal{M}_R\left(\mathbf{x}_{R_r}\right) + n_{RD} \qquad (4)$$

where: i) $\mathcal{M}_R(\cdot)$ is the bit-to-symbol mapping function used at the relays; ii) $\mathbf{x}_{R_r}$ is the $\log_2(N)$ (relay's own) bits for transmission by the relay R_r; iii) $\Omega_R^{(\mathrm{ON})} = \left\{ r = 1, 2, ..., M | \widehat{\mathbf{x}}_S^{(R_r)} = \mathbf{ID}_{R_r} \right\}$ denotes the set of active relays during the information relaying phase; iv) $n_{RD} = n_{RD}^{(\mathrm{a})} + n_{RD}^{(\mathrm{c})}$; and v) $E_{R_r} = \min\{E_R, \mathcal{E}_{R_r}\}$, with $E_R = \tau_R E_{\max}/L + 1$ $(0 < \tau_R \leq L+1)$ being the relay's transmit energy. In fact, E_R is the constant transmit energy with which the relays would preferably transmit when active. However, if this amount of energy is not available in the battery of relay R_r, then it would transmit with the available energy $\mathcal{E}_{R_r}$.

It is worth noting that each relay makes an independent decision on whether to be active or not during the relaying phase. Therefore, if there are no demodulation errors at the relays, since the ID of each relay is unique, only one of the relays will be activated, *i.e.*, $\mathrm{card}\left\{\Omega_R^{(\mathrm{ON})}\right\} = 1$. As a result, in this scenario, (4) reduces to $y_{RD} = \sqrt{E_{R_m}} h'_{R_m D} \mathcal{M}_R\left(\mathbf{x}_{R_m}\right) + n_{RD}$, where $R_r = R_m$ is the (only) active relay, *i.e.*, the relay for which $\mathbf{ID}_{R_m} = \mathbf{x}_S$. On the other hand, if there are demodulation errors at the relays, more than one relay (or indeed no relay) may get activated, *i.e.*, $\Omega_R^{(\mathrm{ON})} \in \{1, ..., M\}$.

C. Demodulation at the Destination

From the received signal y_{RD} given by (4), the source's data and the relay's data can be jointly demodulated at the destination as follows:

$$\left(\widehat{\mathbf{x}}_S^{(D)}, \widehat{\mathbf{x}}_{R_{\widehat{m}}}^{(D)}\right) = \underset{\substack{\widetilde{m} \in \left\{1,2,...,M | \mathbf{ID}_{R_{\widetilde{m}}} = \widetilde{\mathbf{x}}_S^{(D)}\right\} \\ \mathcal{M}_R\left(\widetilde{\mathbf{x}}_{R_{\widetilde{m}}}^{(D)}\right) \in \chi_R}}{\arg\min} \left\{ \Lambda\left(\widetilde{\mathbf{x}}_S^{(D)}, \widetilde{\mathbf{x}}_{R_{\widetilde{m}}}^{(D)}\right) \right\}$$

$$\Lambda\left(\widetilde{\mathbf{x}}_S^{(D)}, \widetilde{\mathbf{x}}_{R_{\widetilde{m}}}^{(D)}\right) = \frac{\left| y_{RD} - \sqrt{E_R} h'_{R_{\widetilde{m}} D} \mathcal{M}_R\left(\widetilde{\mathbf{x}}_{R_{\widetilde{m}}}^{(D)}\right) \right|^2}{N_0} \qquad (5)$$

where $\widehat{\mathbf{x}}_S^{(D)}$ and $\widehat{\mathbf{x}}_{R_{\widehat{m}}}^{(D)}$ denote the estimates of the source's and the relay $R_{\widehat{m}}$'s information bits $\mathbf{x}_S$ and $\mathbf{x}_{R_m}$, respectively, and $\widetilde{\mathbf{x}}_S^{(D)}$ and $\widetilde{\mathbf{x}}_{R_{\widetilde{m}}}^{(D)}$ are the trial bits used in the hypothesis detection problem at the destination.

Note that the demodulator in (5) estimates $R_{\widehat{m}}$ as the only relay which is active. In other words, the relays R_r for $r = 1, 2, ..., M$ with $r \neq \widehat{m}$ are estimated to be silent at the destination. It is also worth noting that in the expression for the demodulator in (5), we have used E_R instead of $E_{R_{\widetilde{m}}}$, the actual energy with which the relay $R_{\widetilde{m}}$ transmits. This is because the destination does not have knowledge of the relay battery's current energy level. More specifically, we have considered an *energy-unaware* demodulator at the destination, i.e., the destination does not have the energy state information of the battery of each relay. Therefore, the destination assumes that the relays when active for transmission, transmits with energy E_R. This leads to a simple demodulation at the destination. In fact, the battery status of a particular relay is known only to that relay, and not to any other nodes in the network. Furthermore, the simulation results in Fig. 3 and further numerical results in Section VII show that using E_R for $E_{R_{\widetilde{m}}}$ is sufficient for achieving a very good performance.

We close this section by noting that wireless-powered DSM (both PS-DSM and ER-DSM) avoids reductions of the aggregate network throughput by allowing each active relay to help the source while forwarding its own data, thus improves the network fairness. Indeed, the fact that the relay's transmit energy is obtained from the source via SWIPT acts as an incentive to encourage the relays to cooperate in forwarding the source's data.

IV. Energy-Recycling Based DSM

As seen earlier, in PS-DSM, only one of the M relays is activated during the information relaying phase. All the remaining $M-1$ relays stay idle, and do not participate in either the relaying or the energy harvesting/information decoding process. Although the inactive relays implicitly contribute to increasing the spectral efficiency of the source, these valuable resources are, in general, under-used. Motivated by this consideration, and in addition to reduce the hardware complexity at the relays, in this section, we propose the ER-DSM protocol. The protocol is illustrated in Fig. 2. In what follows we describe the two transmission phases in ER-DSM: the information broadcasting phase, and the simultaneous information relaying and energy broadcasting phase. It is worth noting that the transmission phases in ER-DSM are slightly different to those of PS-DSM.

[1]In this paper the terms "active" and "inactive" refer to ON and OFF states of the relays with respect to information transmission, respectively. The relays may or may not be harvesting energy.

[2]For simplicity, we consider that the harvested energy at the relays is utilized only for information relaying. The energy spent to demodulate data during the first phase is considered to be negligible.

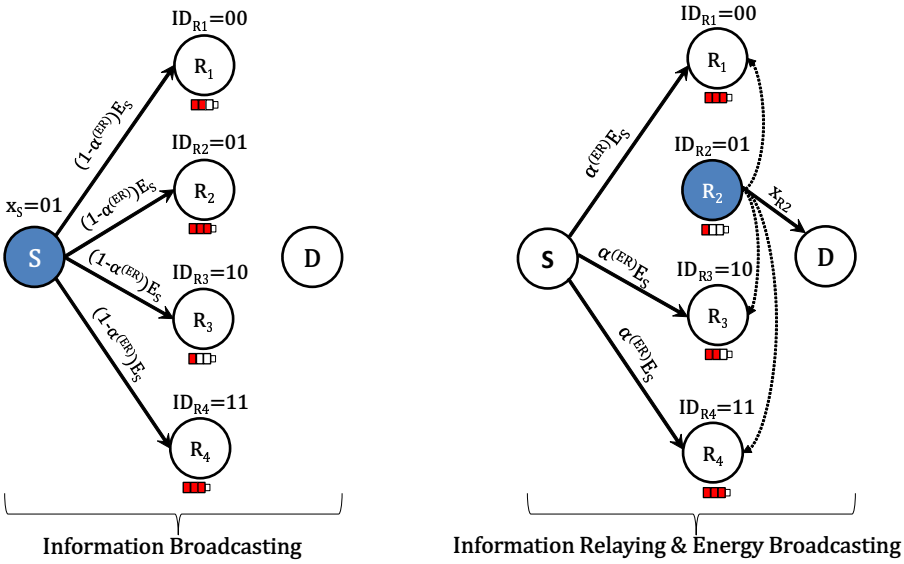

Fig. 2: Illustration of ER-DSM protocol for $M = 4$.

A. Information Broadcasting Phase

In this phase, the source broadcasts its data, *i.e.*, *information symbol*, to the M distributed relays using energy $\left(1-\alpha^{(\mathrm{ER})}\right) E_S$. Accordingly, the information signal received at the relays can be formulated as follows ($r = 1, 2, ..., M$):

$$y_{SR_r} = \sqrt{\left(1-\alpha^{(\mathrm{ER})}\right) E_S} h'_{SR_r} \mathcal{M}_S\left(\mathbf{x}_S\right) + n^{(\mathrm{a})}_{SR_r} + n^{(\mathrm{c})}_{SR_r} \quad (6)$$

Each relay demodulates the signal y_{SR_r} using the ML criterion, as in (2).

B. Simultaneous Information Relaying and Energy Broadcasting Phase

In this phase, similar to Section III-B, one of the relays is activated in accordance with the principle of SM to simultaneously forward the source's estimated data and the (active) relay's own data. The resulting received information signal at the destination can be formulated as in (4). Concurrently during the information transmission from the relays, the source broadcasts an *energy symbol*[3] using energy $\alpha^{(\mathrm{ER})} E_S$ to all those relays that are inactive during the relaying phase. The inactive relays in ER-DSM are in the energy harvesting mode during this phase. As a result, in addition to the energy harvested from the dedicated energy signal broadcasted by the source, the inactive relays can also harvest the energy from the information signal transmitted from the active relay. Therefore, in ER-DSM, the source's energy used to transmit data during the first phase is *recycled*, in part, during the second phase. Furthermore, since the relays do not receive data during this phase, the information signal is not corrupted due to inter-relay interference. Thus, unlike conventional relaying protocols such as successive relaying, the inter-relay interference is beneficial to ER-DSM.

Based on the above considerations, the energy remaining after the energy harvesting phase at each *inactive* relay R_r (i.e., each relay R_r where $r \notin \Omega_R^{(ON)}$) can be formulated as shown in (7). Unlike PS-DSM, in ER-DSM, energy is harvested, as well as spent for information relaying during the second phase. The demodulator at the destination for ER-DSM is same as that for PS-DSM given in (5). By comparing the harvested energy expressions of (3) and (7), the advantage of ER-DSM over PS-DSM can be readily observed. We also note here that in ER-DSM, if $E_{R_r} = 0$ for any inactive relay R_r with $\widehat{\mathbf{x}}_S^{(R_r)} = \mathbf{ID}_{R_r}$, *i.e.*, in the event where the relay that needs to be activated has zero energy in its battery, then that relay will harvest energy in accordance with (7).

With regards to the working principle of ER-DSM, a question naturally arises: *How will the active relay harvest the energy needed for transmission in the subsequent information relaying phase?* The answer to this question is based on the analytical results of [1, Section V], where it has been proven that, *on average*, only one of the relays is active during any given relaying phase in DSM. This result holds even in the presence of possible demodulation errors at the relays. In other words, on average, any given relay R_r is active only once during M relaying phases. Therefore, during the other $M-1$ relaying phases, during which R_r is inactive, it can harvest

[3]In this paper, we use $+1$ as the energy symbol.

$$\mathcal{E}_{R_r} = \max_{i\in\{0,1,\ldots,L+1\}} \left\{ \mathcal{E}^{(i)} : \mathcal{E}^{(i)} < \widetilde{\mathcal{E}}_{R_r} + \eta \left(\left| \sqrt{\alpha^{(\mathrm{ER})} E_S} h'_{SR_r} + \sum_{p\in\Omega_R^{(\mathrm{ON})}} \sqrt{E_{R_p}} h'_{R_p R_r} \mathcal{M}_R\left(\mathbf{x}_{R_p}\right) \right|^2 \right) \right. \quad (7)$$

and accumulate energy in ER-DSM.

Remark 1: The advantage of ER-DSM over PS-DSM is not merely exploiting the inter-relay interference for harvesting additional energy at the relays. Other key differences and potential advantages are as follows. 1) Unlike PS-DSM, ER-DSM does not require complicated power splitting circuitry[4] at any of the M relay nodes. This considerably reduces the complexity and cost of the hardware in the network[5]. 2) The energy harvesting performance of ER-DSM improves considerably when the relays are in close proximity to each other (or clustered). On the other hand, the physical distances between the relays have no effect on the energy harvesting performance of PS-DSM. 3) Finally, the inactive relays in ER-DSM operate either in information decoding mode or in energy harvesting mode at all time instances. Therefore, valuable network resources are utilized to a greater extent compared to PS-DSM.

Remark 2: Note that here we have provided the exposition for an uncoded system; this is mainly in order to keep the mathematical analysis of the system performance tractable. The relay protocol is therefore described based on a symbol-wise perspective. However, the proposed DSM-based SWIPT protocol can be straightforwardly extended to incorporate state-of-the-art channel coding (e.g. turbo or LDPC coding).[6]

V. Markov chain Analytical Model

As illustrated in Section II, we consider a discrete-level battery model with $L+2$ energy states for each of the M relays. For relay R_r ($r = 1, 2, ..., M$), the energy state is denoted as $\mathcal{S}_{R_r}^{(i)}$ if the stored energy at the battery is $\mathcal{E}^{(i)}$. For instance, the state $\mathcal{S}_{R_r}^{(0)}$ indicates that the battery at R_r is empty, and the state $\mathcal{S}_{R_r}^{(L+1)}$ indicates that the battery is fully charged. The transition probability, on the other hand, is denoted as $\mathcal{T}_{R_r}(i,j) = \Pr\left\{\mathcal{S}_{R_r}^{(i)} \rightarrow \mathcal{S}_{R_r}^{(j)}\right\}$, and it is defined as the probability of transitioning from the i-th energy state to the j-th energy state at the battery of R_r.

The charging/discharging behaviour of the relay batteries is modeled using a finite state Markov chain with $L+2$ states ($\mathcal{S}_{R_r}^{(0)}$, $\mathcal{S}_{R_r}^{(1)}$,...,$\mathcal{S}_{R_r}^{(L+1)}$) [15]. In this section, by using a Markov chain model, we first formulate the state transition probability matrix for the battery at the relay R_r, and with the aid of this matrix, we compute the steady-state distribution. Due to space limitations, in this paper we consider only the Markov chain and the performance analysis for ER-DSM. In fact, ER-DSM has been chosen for further analysis due to its particular operating principle. The analysis can be extended to PS-DSM by following a similar mathematical development to that presented here for ER-DSM.

A. Construction of the State Transition Matrix

In general, the state transition probability can be formulated as follows[7]:

$$\begin{aligned}
&\mathcal{T}_{R_r}(i,j) = \left(\frac{1}{M}\right) \sum_{\mathbf{x}_S \in \chi_S} \mathbb{E}_{\mathbf{h}_{SR},\mathbf{h}_{RR}} \left\{\mathcal{T}_{R_r}(i,j;\mathbf{x}_S)\right\} \\
&\mathcal{T}_{R_r}(i,j;\mathbf{x}_S) \\
&= \sum_{\Theta} \left[\mathcal{G}_{R_r}^{(\mathrm{neq})}(i,j;\Theta)\,\overline{\mathcal{Q}}_r(\mathbf{x}_S) + \mathcal{G}_{R_r}^{(\mathrm{eq})}(i,j;\Theta)\,\mathcal{Q}_r(\mathbf{x}_S)\right] \\
&\times \prod_{p \in \Omega_R^{(\mathrm{ON})}(\Theta)} \mathcal{Q}_p(\mathbf{x}_S) \times \prod_{p \in \Omega_R^{(\mathrm{OFF})}(\Theta)} \overline{\mathcal{Q}}_p(\mathbf{x}_S)
\end{aligned} \tag{8}$$

where: i) Θ denotes the set of all independent activation events for all relays except for R_r; ii) $\Omega_R^{(\mathrm{ON})}(\Theta)$ and $\Omega_R^{(\mathrm{OFF})}(\Theta)$ denote the set of active and inactive relays for the event Θ, respectively; iii) $\mathcal{G}_{R_r}^{(\mathrm{neq})}(\cdot,\cdot;\cdot)$ and $\mathcal{G}_{R_r}^{(\mathrm{eq})}(\cdot,\cdot;\cdot)$ are defined as follows:

$$\begin{aligned}
\mathcal{G}_{R_r}^{(\mathrm{neq})}(i,j;\Theta) &= \Pr\left\{\mathcal{S}_{R_r}^{(i)} \rightarrow \mathcal{S}_{R_r}^{(j)} | \widehat{\mathbf{x}}_S^{(R_r)} \neq \mathbf{ID}_{R_r}; \Theta\right\} \\
\mathcal{G}_{R_r}^{(\mathrm{eq})}(i,j;\Theta) &= \Pr\left\{\mathcal{S}_{R_r}^{(i)} \rightarrow \mathcal{S}_{R_r}^{(j)} | \widehat{\mathbf{x}}_S^{(R_r)} = \mathbf{ID}_{R_r}; \Theta\right\}
\end{aligned} \tag{9}$$

and v) $\mathcal{Q}_x(\mathbf{x}_S) = \Pr\left\{\widehat{\mathbf{x}}_S^{(R_x)} = \mathbf{ID}_{R_x} | \mathbf{x}_S\right\}$ denotes the probability that the relay R_x for $x = 1, 2, ..., M$, is activated conditioned upon $\mathbf{x}_S$, *i.e.*, the probability that the symbol demodulated at R_x is $\mathbf{ID}_{R_x}$ by assuming that the source has transmitted $\mathbf{x}_S$, and $\overline{\mathcal{Q}}_x(\mathbf{x}_S) = 1 - \Pr\left\{\widehat{\mathbf{x}}_S^{(R_x)} = \mathbf{ID}_{R_x} | \mathbf{x}_S\right\}$. Note that (8) follows by using Bayes' rule by taking into account that $\mathcal{T}_{R_r}(i,j;\mathbf{x}_S)$ depends on the energy states of the relay R_r and not on the energy states of relay R_p. This is because the transmitted energy from the relays are considered to be constant in ER-DSM. Furthermore, in ER-DSM, the relay is active (for transmission) if $\widehat{\mathbf{x}}_S^{(R_x)} = \mathbf{ID}_{R_x} | \mathbf{x}_S$ and inactive if $\widehat{\mathbf{x}}_S^{(R_x)} \neq \mathbf{ID}_{R_x} | \mathbf{x}_S$.

Using the union-bound method, $\Pr\left\{\widehat{\mathbf{x}}_S^{(R_x)} \neq \mathbf{ID}_{R_x} | \mathbf{x}_S\right\}$ can be formulated as follows [1], [44]:

$$\begin{aligned}
&\Pr\left\{\widehat{\mathbf{x}}_S^{(R_x)} = \mathbf{ID}_{R_x} | \mathbf{x}_S\right\} \\
&\approx \begin{cases}
Q\left(\sqrt{\frac{\left(1-\alpha^{(\mathrm{ER})}\right)E_S}{2N_0} |d_S(\mathbf{ID}_{R_x})|^2 |h'_{SR_x}|^2}\right) & \text{if } \mathbf{x}_S \neq \mathbf{ID}_{R_x} \\
1 - \beta_a Q\left(\sqrt{2\beta_b \frac{\left(1-\alpha^{(\mathrm{ER})}\right)E_S}{N_0} |h'_{SR_x}|^2}\right) & \text{if } \mathbf{x}_S = \mathbf{ID}_{R_x}
\end{cases}
\end{aligned} \tag{10}$$

where $d_S(\mathbf{ID}_{R_x}) = \mathcal{M}_S(\mathbf{x}_S) - \mathcal{M}_S(\mathbf{ID}_{R_x})$, and β_a and β_b are constants that depend on the employed modulation scheme. For instance, if PSK is being used $\beta_a = \beta_b = 1$ for $M = 2$, and $\beta_a = 2$ and $\beta_b = \sin^2(\pi/M)$ for $M > 2$.

[4]The power splitters are also constrained by efficiency losses due to hardware non-linearities.

[5]For ER-DSM, an antenna switching mechanism at the symbol-level is required at the relay nodes to switch between the energy harvesting mode and the information decoding mode.

[6]In the presence of channel coding, since the relays might not have sufficient computational capabilities for exploiting the channel code, they would have the option of simply performing demodulation (demodulate-and-forward relaying). The destination, on the other hand, may exploit channel coding – this would involve buffering the frame of received signals and forming the relevant log-likelihood ratios (LLRs) for iterative decoding. In the case where the relays also perform channel decoding, the broadcasting and relaying phases may each be considered as lasting for an entire coded frame.

[7]$\mathbf{h}_{SR}$, $\mathbf{h}_{RR}$ and $\mathbf{h}_{RD}$ are short-hands used to denote all the source-to-relay, relay-to-relay and the relay-to-destination channels, respectively.

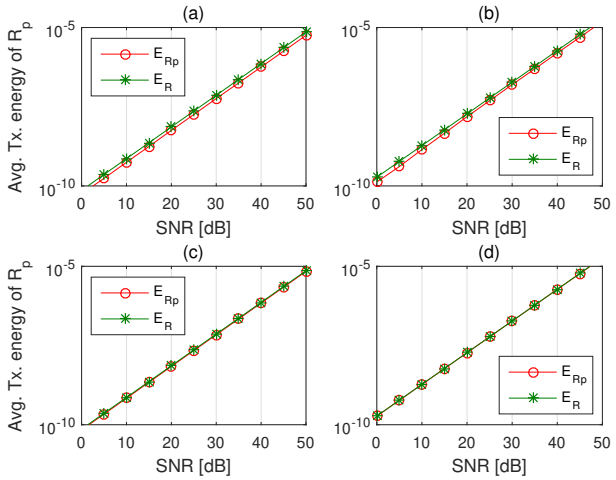

Fig. 3: Illustration of accuracy of the approximation in *Remark 3* (Monte Carlo simulations) with $N = 2$ and $h'_{XY} = h_{XY}$ for all node pairs (X,Y). (a) $M = 2$; $\kappa_R = 2$; $L = 10$; and $\tau_R = 5$. (b) $M = 2$; $\kappa_R = 10$; $L = 100$; and $\tau_R = 20$. (c) $M = 4$; $\kappa_R = 2$; $L = 10$; and $\tau_R = 5$. (d) $M = 4$; $\kappa_R = 10$; $L = 100$; and $\tau_R = 20$.

Remark 3: Strictly speaking, the active relay's transmit energy $E_{R_p} = \min\left\{E_R, \mathcal{E}_{R_p}\right\}$ is a discrete RV as the residual energy $\mathcal{E}_{R_p}$ can take any value from $\mathcal{E}^{(0)}$ to $\mathcal{E}^{(L+1)}$. Note that, however, E_R is a constant. In the computation of transition probabilities, to simplify our analysis, we will approximate E_{R_p} as $E_{R_p} \approx E_R$. We justify this approximation using Fig. 3, where we have compared using Monte Carlo simulations E_{R_p} against E_R for various system setups. It can be clearly observed that E_{R_p} provides a tight approximation to E_R, and hence, this result has been used in the subsequent analysis. In fact, this approximation considerably simplifies our derivations and leads to a a relatively simple closed-form solution to the transition probabilities.

The transition probability in (8) can be evaluated by considering following four general cases [17]:

Case 1 *($\mathcal{T}_{R_r}(i,i;\mathbf{x}_S)$; $0 \le i \le L+1$):* In this case, the state of the battery at relay R_r remains unchanged. This means that zero energy is harvested at R_r during the energy broadcasting phase of ER-DSM.

In order to evaluate $\mathcal{T}_{R_r}(i,i;\mathbf{x}_S)$, let us first consider the scenario where $i = L+1$, *i.e.*, the battery remains fully charged. In more detail, the battery at the relay R_r was fully charged prior to the energy broadcasting phase, and therefore R_r cannot harvest any more energy. Accordingly, $\mathcal{G}^{(\text{neq})}_{R_r}(L+1,L+1;\Theta)$ and $\mathcal{G}^{(\text{eq})}_{R_r}(L+1,L+1;\Theta)$ can be formulated as follows:

$$\begin{aligned}&\mathcal{G}^{(\text{neq})}_{R_r}(L+1,L+1;\Theta)\\ &= \Pr\left\{\eta\left|\sqrt{\alpha^{(\text{ER})}E_S}h'_{SR_r} + \mathcal{H}_{RR_r}(\Theta)\right|^2 > 0\right\} = 1 \quad (11)\\ &\mathcal{G}^{(\text{eq})}_{R_r}(L+1,L+1;\Theta) \overset{(a)}{=} 0\end{aligned}$$

where $\mathcal{H}_{RR_r}(\Theta) = \sum_{p\in\Omega^{(\text{ON})}_R(\Theta)} \sqrt{E_R}h'_{R_pR_r}\mathcal{M}_R\left(\mathbf{x}_{R_p}\right)$, and (a) follows because when the relay R_r is active, *i.e.*, when $\widehat{\mathbf{x}}^{(R_r)}_S = \mathbf{ID}_{R_r}$, the battery will be discharged, and hence, it will not remain in the same state.

On the other hand, when $i = 0$, the battery remains empty. More specifically, the battery was empty prior to the energy broadcasting phase, and remains so as the harvested energy is lower than the first energy level $\mathcal{E}^{(1)}$. Accordingly, $\mathcal{G}^{(\text{neq})}_{R_r}(0,0;\Theta)$ and $\mathcal{G}^{(\text{eq})}_{R_r}(0,0;\Theta)$ can be formulated as follows:

$$\begin{aligned}&\mathcal{G}^{(\text{neq})}_{R_r}(0,0;\Theta) = \mathcal{G}^{(\text{eq})}_{R_r}(0,0;\Theta)\\ &= \Pr\left\{\eta\left|\sqrt{\alpha^{(\text{ER})}E_S}h'_{SR_r} + \mathcal{H}_{RR_r}(\Theta)\right|^2 < \mathcal{E}^{(1)}\right\} \quad (12)\\ &= F_{\mathcal{I}_{R_r}(\Theta)}\left(\frac{\mathcal{E}^{(1)}}{\eta}\right)\end{aligned}$$

where $\mathcal{I}_{R_r}(\Theta) = \left|\sqrt{\alpha^{(\text{ER})}E_S}h'_{SR_r} + \mathcal{H}_{RR_r}(\Theta)\right|^2$. The

$$\begin{aligned}\mathcal{T}_{R_r}(i,i;\mathbf{x}_S;i=0) &= \sum_{\Theta} F_{\mathcal{I}_{R_r}(\Theta)}\left(\frac{\mathcal{E}^{(1)}}{\eta}\right) \times \prod_{p\in\Omega^{(\text{ON})}_R(\Theta)} \mathcal{Q}_p(\mathbf{x}_S) \times \prod_{p\in\Omega^{(\text{OFF})}_R(\Theta)} \overline{\mathcal{Q}}_p(\mathbf{x}_S)\\ \mathcal{T}_{R_r}(i,i;\mathbf{x}_S;i=L+1) &= \sum_{\Theta} \overline{\mathcal{Q}}_r(\mathbf{x}_S) \times \prod_{p\in\Omega^{(\text{ON})}_R(\Theta)} \mathcal{Q}_p(\mathbf{x}_S) \times \prod_{p\in\Omega^{(\text{OFF})}_R(\Theta)} \overline{\mathcal{Q}}_p(\mathbf{x}_S) \quad (13)\\ \mathcal{T}_{R_r}(i,i;\mathbf{x}_S;0<i<L+1) &= \sum_{\Theta} F_{\mathcal{I}_{R_r}(\Theta)}\left(\frac{\mathcal{E}^{(1)}}{\eta}\right) \times \overline{\mathcal{Q}}_r(\mathbf{x}_S) \times \prod_{p\in\Omega^{(\text{ON})}_R(\Theta)} \mathcal{Q}_p(\mathbf{x}_S) \times \prod_{p\in\Omega^{(\text{OFF})}_R(\Theta)} \overline{\mathcal{Q}}_p(\mathbf{x}_S)\end{aligned}$$

above result, in particular, follows for $\mathcal{G}_{R_r}^{(\mathrm{eq})}(0,0;\Theta)$ by noting that even though $\widehat{\mathbf{x}}_S^{(R_r)} \neq \mathbf{ID}_{R_r}$, the relay R_r will not be activated (for transmission) as it has zero energy in its battery. Therefore, relay R_r will be in charging mode.

By following a similar line of thought to the above for $i = 1, 2, ..., L$, *i.e.*, when the non-empty and non-full battery remains unchanged, we obtain $\mathcal{G}_{R_r}^{(\mathrm{neq})}(i,i;\Theta) = F_{\mathcal{I}_{R_r}(\Theta)}\left(\frac{\mathcal{E}^{(1)}}{\eta}\right)$ and $\mathcal{G}_{R_r}^{(\mathrm{eq})}(i,i;\Theta) = 0$. From the above results for $\mathcal{G}_{R_r}^{(\mathrm{neq})}(\cdot,\cdot;\Theta)$ and $\mathcal{G}_{R_r}^{(\mathrm{eq})}(\cdot,\cdot;\Theta)$, the transition probability $\mathcal{T}_{R_r}(\cdot,\cdot;\cdot)$ when the battery remains unchanged can be formulated using (8) as shown in (13).

Finally, $\mathcal{T}_{R_r}(i,j;\mathbf{x}_S;\cdot) = \mathbb{E}_{\mathbf{h}_{SR},\mathbf{h}_{RR}}\{\mathcal{T}_{R_r}(i,j;\mathbf{x}_S;\cdot)\}$ can be computed as shown in (14), where: i) $\Upsilon_{R_x} = \frac{(1-\alpha^{(\mathrm{ER})})E_S}{4N_0 L_{SR_x}}|d_S(\mathbf{ID}_{R_x})|^2$; ii) $\xi_{R_x} = \beta_b \frac{(1-\alpha^{(\mathrm{ER})})E_S}{N_0 L_{SR_x}}$; iii) $\sigma^2_{\mathcal{Z}_{R_r}}(\Theta) = \frac{\alpha^{(\mathrm{ER})}E_S}{L_{SR_r}} + \sum\limits_{p\in\Omega_R^{(\mathrm{ON})}(\Theta)} \frac{E_R}{L_{R_pR_r}}$; iv) $\omega_R^{(\mathrm{ON})}(\Theta) = \mathrm{card}\left\{\Omega_R^{(\mathrm{ON})}(\Theta)\right\}$; v) $\omega_{R,\mathrm{neq}}^{(\mathrm{ON})}(\Theta) = \mathrm{card}\left\{\Omega_{R,\mathrm{neq}}^{(\mathrm{ON})}(\Theta)\right\}$ with $\Omega_{R,\mathrm{neq}}^{(\mathrm{ON})}(\Theta) = \left\{p \in \Omega_R^{(\mathrm{ON})}(\Theta) \,|\mathbf{x}_S \neq \mathbf{ID}_{R_p}\right\}$; vi) $\omega_{R,\mathrm{eq}}^{(\mathrm{OFF})}(\Theta) = \mathrm{card}\left\{\Omega_{R,\mathrm{eq}}^{(\mathrm{OFF})}(\Theta)\right\}$ with $\Omega_{R,\mathrm{eq}}^{(\mathrm{OFF})}(\Theta) = \left\{p \in \Omega_R^{(\mathrm{OFF})}(\Theta) \,|\mathbf{x}_S = \mathbf{ID}_{R_p}\right\}$; vii) $\mathcal{K}_R(\Theta) = (1/N)^{\omega_R^{(\mathrm{ON})}(\Theta)} \times (1/2)^{\omega_{R,\mathrm{neq}}^{(\mathrm{ON})}(\Theta)} \times (\beta_a/2)^{\omega_{R,\mathrm{eq}}^{(\mathrm{OFF})}(\Theta)}$; viii) (a), (b) and $(c1)$ follows from (10) by applying the Chernoff bound [44], and with the aid of the high-SNR approximations $1 - Q(\sqrt{x}) \to 1$ and $1 + (E_S/N_0)x \approx (E_S/N_0)x$. In $(c2)$, in order to bypass the statistical dependence of the first and the second terms in the third line of (13), and to formulate a closed-form solution, we have used Fortuin-Kasteleyn-Ginibre (FKG) inequality for an increasing and a decreasing RV [45]. In addition, we have applied the definition of exponential RV and have exploited the independence of h'_{SR_r}, h_{SR_p} and $h'_{R_pR_r}$ to obtain the closed-form solutions in (14).

Case 2 *($\mathcal{T}_{R_r}(i,j;\mathbf{x}_S)$; $0 \leq i < j < L+1$):* In this case, the empty or the non-empty battery at the relay R_r harvests energy to become partially charged. Accordingly, the transition probability can be formulated as shown in (15), where (a) in (15) follows by using arguments similar to Case 1. For brevity, the complete mathematical development is not shown here.

Case 3 *($\mathcal{T}_{R_r}(i,L+1;\mathbf{x}_S)$; $0 \leq i < L+1$):* In this case, the battery at relay R_r harvests energy to become fully charged. The state of the battery prior to harvesting is either empty, *i.e.*, $i = 0$, or partially charged, *i.e.*, $1 \leq i < L+1$. Accordingly, the final expressions for the transition probability can be formulated as shown in (16).

Case 4 *($\mathcal{T}_{R_r}(i,j;\mathbf{x}_S)$; $j < i; i \neq j$):* In accordance with the proposed ER-DSM protocol, the relay R_r with non-empty battery activates (and discharges energy) for information relaying when the demodulated data at R_r coincides with its ID, *i.e.*, $\widehat{\mathbf{x}}_S^{(R_r)} = \mathbf{ID}_{R_r}$. Accordingly, $\mathcal{G}_{R_r}^{(\mathrm{neq})}(i,j)$ and $\mathcal{G}_{R_r}^{(\mathrm{eq})}(i,j)$ for $j < i$ and $i \neq 0$ can be formulated as follows:

$$\begin{aligned} &\mathcal{G}_{R_r}^{(\mathrm{neq})}(i,j) \overset{(a)}{=} 0 \\ &\mathcal{G}_{R_r}^{(\mathrm{eq})}(i,j) \overset{(b)}{=} \rho(i,\tau_R)\,\overline{\delta}(j,i-\tau_R) + \overline{\rho}(i,\tau_R)\,\overline{\delta}(j,0) \end{aligned} \tag{17}$$

where: i) $\overset{(a)}{=}$ follows because when the relay R_r is OFF, the battery will not discharged (it will either be charged or remains in the same state); and ii) $\overset{(b)}{=}$ follows because when the relay R_r is ON, if $\tau_R < i$, *i.e.*., if index of the energy level with which the relay R_r transmits is less than the index of the current energy level, the battery discharges energy $\mathcal{E}^{(\tau_R)}$ and jumps to the energy level $\mathcal{E}^{(j)}$ from $\mathcal{E}^{(i)}$. On the other hand, if $\tau_R > i$, the battery discharges to the zero level. It is also worth noting that, unlike previous cases, in this case, the activation events at other relays does not effect the energy state of R_r, *i.e.*, $\mathcal{T}_{R_r}(i,j;\mathbf{x}_S)$ is independent of Θ.

Accordingly, the transition probability can be formulated as

$$\begin{aligned}
\mathcal{T}_{R_r}(i,i;\mathbf{x}_S;i=0) &\overset{(a)}{\approx} \sum_{\Theta} \mathcal{K}_R(\Theta) \times \left(1 - \exp\left(-\frac{\mathcal{E}^{(1)}}{\eta\sigma^2_{\mathcal{Z}_{R_r}}(\Theta)}\right)\right) \times \prod_{p\in\Omega_{R,\mathrm{neq}}^{(\mathrm{ON})}(\Theta)} (\Upsilon_{R_p})^{-1} \prod_{p\in\Omega_{R,\mathrm{eq}}^{(\mathrm{OFF})}(\Theta)} (\xi_{R_r})^{-1} \\
\mathcal{T}_{R_r}(i,i;\mathbf{x}_S;i=L+1) &\overset{(b)}{\approx} \sum_{\Theta} \mathcal{K}_R(\Theta) \times \left(\frac{2\xi_{R_r}}{\beta_a}\right)^{-\overline{\delta}\left(|d_S(\mathbf{ID}_{R_r})|^2,0\right)} \times \prod_{p\in\Omega_{R,\mathrm{neq}}^{(\mathrm{ON})}(\Theta)} (\Upsilon_{R_p})^{-1} \times \prod_{p\in\Omega_{R,\mathrm{eq}}^{(\mathrm{OFF})}(\Theta)} (\xi_{R_r})^{-1} \\
\mathcal{T}_{R_r}(i,i;\mathbf{x}_S;0<i<L+1) &\overset{(c1)}{\approx} \sum_{\Theta} F_{\mathcal{I}_{R_r}(\Theta)}\left(\frac{\mathcal{E}^{(1)}}{\eta}\right) \times \left(\frac{\beta_a}{2}\exp\left(-\beta_b\frac{(1-\alpha^{(\mathrm{ER})})E_S}{N_0}|h'_{SR_r}|^2\right)\right)^{\overline{\delta}\left(|d_S(\mathbf{ID}_{R_r})|^2,0\right)} \\
&\quad \times \prod_{p\in\Omega_R^{(\mathrm{ON})}(\Theta)} \mathcal{Q}_p(\mathbf{x}_S) \times \prod_{p\in\Omega_R^{(\mathrm{OFF})}(\Theta)} \overline{\mathcal{Q}}_p(\mathbf{x}_S) \\
&\overset{(c2)}{\leq} \sum_{\Theta} \mathcal{K}_R(\Theta) \times \left(1 - \exp\left(-\frac{\mathcal{E}^{(1)}}{\eta\sigma^2_{\mathcal{Z}_{R_r}}(\Theta)}\right)\right) \times \left(\frac{2\xi_{R_r}}{\beta_a}\right)^{-\overline{\delta}\left(|d_S(\mathbf{ID}_{R_r})|^2,0\right)} \times \prod_{p\in\Omega_{R,\mathrm{neq}}^{(\mathrm{ON})}(\Theta)} (\Upsilon_{R_p})^{-1} \times \prod_{p\in\Omega_{R,\mathrm{eq}}^{(\mathrm{OFF})}(\Theta)} (\xi_{R_r})^{-1}
\end{aligned} \tag{14}$$

follows:

$$\begin{aligned}&\mathcal{T}_{R_r}\left(i,j;\mathbf{x}_S;j<i;i\neq j\right)\\&=\left[\rho\left(i,\tau_R\right)\overline{\delta}\left(j,i-\tau_R\right)+\overline{\rho}\left(i,\tau_R\right)\overline{\delta}\left(j,0\right)\right]\\&\times\Pr\left\{\widehat{\mathbf{x}}_S^{(R_r)}=\mathbf{ID}_{R_r}|\mathbf{x}_S\right\}\\&\mathcal{T}_{R_r}\left(i,j;\mathbf{x}_S;j<i;i\neq j\right)\\&\approx\frac{1}{2}\left[\rho\left(i,\tau_R\right)\overline{\delta}\left(j,i-\tau_R\right)+\overline{\rho}\left(i,\tau_R\right)\overline{\delta}\left(j,0\right)\right]\\&\times\left(\Upsilon_{R_r}\right)^{-\delta\left(|d_S(\mathbf{ID}_{R_r})|^2,0\right)}\end{aligned}\tag{18}$$

Finally, the state transition matrix $\mathbf{T}_{R_r}=\left[\mathcal{T}_{R_r}\left(i,j\right)\right]_{i,j=0}^{L+1}$ of dimension $(L+2)\times(L+2)$ at the relay R_r for $r=1,2,...,M$ can be constructed with the aid of (8), (14), (15), (16) and (18). It is worth noting that for independent identically distributed (i.i.d.) fading channels $\mathbf{T}_{R_1}=\mathbf{T}_{R_2}=...=\mathbf{T}_{R_M}=\mathbf{T}$.

For the sake of illustration, in Fig. 4, we show the state transition diagram of the Markov chain depicting the possible states of the battery at the relay R_r, as well as the transitions between the states, for the case when $L=2$ and $\tau_R=2$. The corresponding state transition matrix $\mathbf{T}_{R_r}$ has also been provided in Fig. 4.

B. Computation of steady-state distribution

The state transition matrix $\mathbf{T}_{R_r}$ is irreducible[8] and row stochastic[9] (see Fig. 4). Therefore, if $\mathbf{\Psi}_{R_r}=\left[\Psi_{R_r}^{(0)},\Psi_{R_r}^{(1)},...,\Psi_{R_r}^{(L+1)}\right]$ denotes the vector of stead-state probabilities, then there exists a unique solution such that $\mathbf{\Psi}_{R_r}\mathbf{T}_{R_r}=\mathbf{\Psi}_{R_r}$. By solving this equation, we obtain the steady-state distribution of finite-state Markov chain process at the battery of relay R_r $(r=1,2,...,M)$ as follows [15]:

$$\mathbf{\Psi}_{R_r}=\left(\mathbf{T}_{R_r}-\mathbf{I}+\mathbf{B}\right)^{-1}\mathbf{b}\tag{19}$$

where $\mathbf{I}$ is the identity matrix, and $\mathbf{B}$ and $\mathbf{b}$ are matrices of ones having dimensions $(L+2)\times(L+2)$ and $(L+2)\times1$, respectively.

In Fig. 5a and Fig. 5b, the steady state distribution obtained using the analytical framework of this section are compared against those obtained via Monte Carlo simulations. These figures confirm that the proposed analytical model is very tight with respect to the actual distribution[10], thus validating the accuracy of the approximations used. Therefore, in the next section, we utilize the above results for the error performance evaluation of ER-DSM.

[8]A Markov chain is irreducible if the present state can reach any other state in finite number of time steps [46].

[9]The transition probability matrix of the Markov chain is row stochastic if the sum of all the elements in a row is one. In other words, the sum of the transition probabilities from the present state to all the other states is one [46].

[10]The tightness of the analytical results to the Monte Carlo simulation results for the error probability curves in Section VII further justifies the approximations used in Section V for computing the steady-state distribution.

$$\begin{aligned}&\mathcal{T}_{R_r}\left(i,j;\mathbf{x}_S;0\leq i<j<L+1\right)=\sum_{\Theta}\left(F_{\mathcal{I}_{R_r}(\Theta)}\left(\frac{\mathcal{E}^{(j+1)}-\mathcal{E}^{(i)}}{\eta}\right)-F_{\mathcal{I}_{R_r}(\Theta)}\left(\frac{\mathcal{E}^{(j)}-\mathcal{E}^{(i)}}{\eta}\right)\right)\\&\qquad\times\left(\overline{\mathcal{Q}}_r\left(\mathbf{x}_S\right)\overline{\delta}\left(i,0\right)+\mathcal{Q}_r\left(\mathbf{x}_S\right)\right)\times\prod_{p\in\Omega_R^{(\mathrm{ON})}(\Theta)}\mathcal{Q}_p\left(\mathbf{x}_S\right)\times\prod_{p\in\Omega_R^{(\mathrm{OFF})}(\Theta)}\overline{\mathcal{Q}}_p\left(\mathbf{x}_S\right)\\&\mathcal{T}_{R_r}\left(i,j;\mathbf{x}_S;0\leq i<j<L+1\right)\overset{(a)}{\approx}\sum_{\Theta}\mathcal{K}_R\left(\Theta\right)\times\left(\exp\left(-\frac{\mathcal{E}^{(j)}-\mathcal{E}^{(i)}}{\eta\sigma^2_{\mathcal{Z}_{R_r}}(\Theta)}\right)-\exp\left(-\frac{\mathcal{E}^{(j+1)}-\mathcal{E}^{(i)}}{\eta\sigma^2_{\mathcal{Z}_{R_r}}(\Theta)}\right)\right)\\&\times\left(\left(\frac{2\xi_{R_r}}{\beta_a}\right)^{-\overline{\delta}\left(|d_S(\mathbf{ID}_{R_r})|^2,0\right)}\overline{\delta}\left(i,0\right)+\left(\Upsilon_{R_r}\right)^{-\delta\left(|d_S(\mathbf{ID}_{R_r})|^2,0\right)}\right)\times\prod_{p\in\Omega_{R,\mathrm{neq}}^{(\mathrm{ON})}(\Theta)}\left(\Upsilon_{R_p}\right)^{-1}\times\prod_{p\in\Omega_{R,\mathrm{eq}}^{(\mathrm{OFF})}(\Theta)}\left(\xi_{R_r}\right)^{-1}\end{aligned}\tag{15}$$

$$\begin{aligned}&\mathcal{T}_{R_r}\left(i,L+1;\mathbf{x}_S;0\leq i<L+1\right)=\sum_{\Theta}\left(1-F_{\mathcal{I}_{R_r}(\Theta)}\left(\frac{E_{\max}-\mathcal{E}^{(i)}}{\eta}\right)\right)\\&\qquad\times\left(\overline{\mathcal{Q}}_r\left(\mathbf{x}_S\right)\overline{\delta}\left(i,0\right)+\mathcal{Q}_r\left(\mathbf{x}_S\right)\right)\times\prod_{p\in\Omega_R^{(\mathrm{ON})}(\Theta)}\mathcal{Q}_p\left(\mathbf{x}_S\right)\times\prod_{p\in\Omega_R^{(\mathrm{OFF})}(\Theta)}\overline{\mathcal{Q}}_p\left(\mathbf{x}_S\right)\\&\mathcal{T}_{R_r}\left(i,L+1;\mathbf{x}_S;0\leq i<L+1\right)\approx\sum_{\Theta}\mathcal{K}_R\left(\Theta\right)\times\exp\left(-\frac{E_{\max}-\mathcal{E}^{(i)}}{\eta}\right)\\&\times\left(\left(\frac{2\xi_{R_r}}{\beta_a}\right)^{-\overline{\delta}\left(|d_S(\mathbf{ID}_{R_r})|^2,0\right)}\overline{\delta}\left(i,0\right)+\left(\Upsilon_{R_r}\right)^{-\delta\left(|d_S(\mathbf{ID}_{R_r})|^2,0\right)}\right)\times\prod_{p\in\Omega_{R,\mathrm{neq}}^{(\mathrm{ON})}(\Theta)}\left(\Upsilon_{R_p}\right)^{-1}\times\prod_{p\in\Omega_{R,\mathrm{eq}}^{(\mathrm{OFF})}(\Theta)}\left(\xi_{R_r}\right)^{-1}\end{aligned}\tag{16}$$

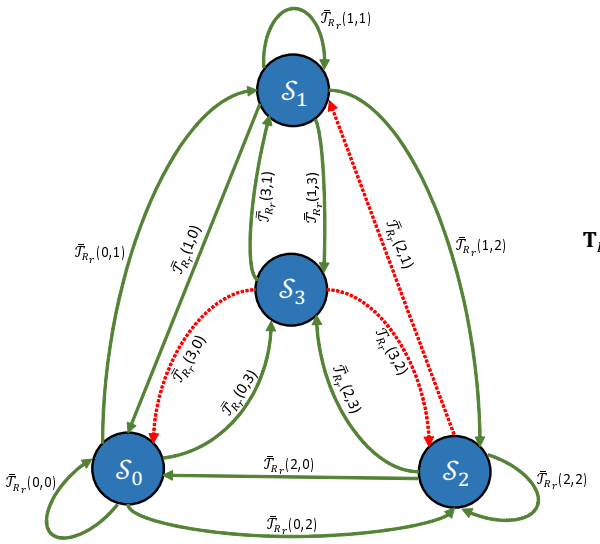

$$\mathbf{T}_{R_r} = \begin{bmatrix} \bar{\mathcal{T}}_{R_r}(0,0) & \bar{\mathcal{T}}_{R_r}(0,1) & \bar{\mathcal{T}}_{R_r}(0,2) & \bar{\mathcal{T}}_{R_r}(0,3) \\ \bar{\mathcal{T}}_{R_r}(1,0) & \bar{\mathcal{T}}_{R_r}(1,1) & \bar{\mathcal{T}}_{R_r}(1,2) & \bar{\mathcal{T}}_{R_r}(1,3) \\ \bar{\mathcal{T}}_{R_r}(2,0) & 0 & \bar{\mathcal{T}}_{R_r}(2,2) & \bar{\mathcal{T}}_{R_r}(2,3) \\ 0 & \bar{\mathcal{T}}_{R_r}(3,1) & 0 & \bar{\mathcal{T}}_{R_r}(3,3) \end{bmatrix}$$

Fig. 4: The state transition diagram of the Markov chain in ER-DSM, depicting the possible states of the battery at the relay R_r, as well as the transitions between the states. The illustration is for the case when $L = 2$ and $\tau_R = 2$. The dotted lines show the transitions with zero probability (see Case 4). The corresponding state transition matrix $\mathbf{T}_{R_r}$ is also shown.

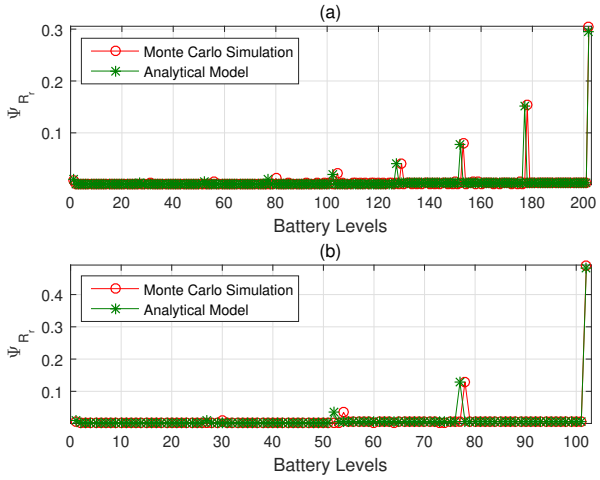

Fig. 5: Comparison of the Monte Carlo simulation and the analytical model for the steady-state distribution. The following parameters are considered: (a) $M = 2$; $N = 4$; $\kappa_R = 2$; $L = 200$; and $\tau_R = 25$. (b) $M = 4$; $N = 2$; $\kappa_R = 10$; $L = 100$; and $\tau_R = 25$. In both (a) and (b), $h'_{XY} = h_{XY}$ for all node pairs (X,Y).

VI. Error Probability Analysis of ER-DSM

In this section, we derive mathematical expressions for computing the error performance of the proposed ER-DSM protocol which employs the demodulator in (5). The general methodology used in this paper to compute the error probability is similar to that of [1], *i.e.*, we first compute the pairwise error probability (PEP)[11] which is conditioned upon the source-to-relay ($\mathbf{h}_{SR}$) and the relay-to-destination ($\mathbf{h}_{RD}$) channels. Then, the average symbol error probability (ASEP) is computed by deconditioning the PEP with respect to $\mathbf{h}_{SR}$ and $\mathbf{h}_{RD}$. Finally, the average symbol error probability (ASEP) is computed from the APEP with the aid of the union bound method.

[11]PEP $(X \to Y)$ is defined as the error probability of deciding on the data symbol Y when X is the actual transmitted symbol, and when X and Y are the only symbols to consider.

A. Computation of the ASEP

Let $\mathbf{x}^{(D)} = \left(\mathbf{x}_S^{(D)}, \overline{\mathbf{x}}_{R_1}^{(D)}, \overline{\mathbf{x}}_{R_2}^{(D)}, ..., \overline{\mathbf{x}}_{R_M}^{(D)}\right)$ and $\widetilde{\mathbf{x}}^{(D)} = \left(\widetilde{\mathbf{x}}_S^{(D)}, \mathcal{N}, ..., \widetilde{\mathbf{x}}_{R_{\widetilde{m}}}^{(D)}, ..., \mathcal{N}\right)$ be the actual transmitted and demodulated symbol vectors, respectively, where $\overline{\mathbf{x}}_{R_r}^{(D)} \in \left\{\mathbf{x}_{R_r}^{(D)}, \mathcal{N}\right\}$ with $\mathcal{N}$ being a notation introduced to denote the OFF (inactive) state of the relays, and $R_{\widetilde{m}}$ is that unique relay satisfying $\mathbf{ID}_{R_{\widetilde{m}}} = \widetilde{\mathbf{x}}_S^{(D)}$. We emphasize that due to possible demodulation errors at the relays, more than one relay, or no relay, may be active. In the ideal scenario where there are no errors at the relays, only one of the relays will be active. In any case, the demodulator in (5) will jointly estimate the source's data, which gives the estimate of the active relay, and the data transmitted from that particular active relay. All the other relays are estimated to be silent (inactive) at the destination.

Accordingly, the PEP conditioned on $\mathbf{h}_{SR}$, $\mathbf{h}_{RD}$ and $\mathbf{n}_{RD}$ can be formulated as shown in (20), where $\Pr\left\{\mathbf{x}^{(D)}|\mathbf{h}_{RD}\right\}$ denotes the probability of transmission of the symbol vector $\mathbf{x}^{(D)}$ conditioned upon $\mathbf{h}_{RD}$. In the later part of this section, the expression for computing $\Pr\left\{\mathbf{x}^{(D)}|\mathbf{h}_{RD}\right\}$ has been formulated; and $\Delta\left(\mathbf{x}^{(D)},\widetilde{\mathbf{x}}^{(D)}\right)$ is defined as follows:

$$\begin{aligned}
&\Delta\left(\mathbf{x}^{(D)},\widetilde{\mathbf{x}}^{(D)}\right)=\Lambda\left(\widetilde{\mathbf{x}}^{(D)}\right)-\Lambda\left(\mathbf{x}^{(D)}\right)\\
&\overset{(a)}{=}\frac{\left|\sum\limits_{r\in\Omega_R^{(\mathrm{ON})}\left(\mathbf{x}^{(D)}\right)}\sqrt{E_R}\mathcal{A}_{R_r}-\sqrt{E_R}\widetilde{\mathcal{A}}_{R_{\widetilde{m}}}\right|^2}{N_0}\\
&\quad-\frac{\left|\sum\limits_{r\in\Omega_R^{(\mathrm{ON})}\left(\mathbf{x}^{(D)}\right)}\sqrt{E_R}\mathcal{A}_{R_r}-\sqrt{E_R}\mathcal{A}_{R_m}\right|^2}{N_0}\\
&\quad+\frac{2\mathrm{Re}\left\{\left(\sum\limits_{r\in\Omega_R^{(\mathrm{ON})}\left(\mathbf{x}^{(D)}\right)}\sqrt{E_R}\mathcal{A}_{R_r}-\sqrt{E_R}\widetilde{\mathcal{A}}_{R_{\widetilde{m}}}\right)n_{RD}^*\right\}}{N_0}\\
&\quad-\frac{2\mathrm{Re}\left\{\left(\sum\limits_{r\in\Omega_R^{(\mathrm{ON})}\left(\mathbf{x}^{(D)}\right)}\sqrt{E_R}\mathcal{A}_{R_r}-\sqrt{E_R}\mathcal{A}_{R_m}\right)n_{RD}^*\right\}}{N_0}
\end{aligned}\tag{21}$$

where (a) follows by inserting $y_{RD}=\sum\limits_{r\in\Omega_R^{(\mathrm{ON})}\left(\mathbf{x}^{(D)}\right)}\sqrt{E_{R_r}}h'_{R_rD}\mathcal{M}_R\left(\mathbf{x}_{R_r}\right)$ in the expression for $\Lambda\left(\cdot\right)$. For convenience, we have also introduced the notations $\mathcal{A}_{R_m}=h'_{R_mD}\mathcal{M}\left(\mathbf{x}_{R_m}\right)$ and $\widetilde{\mathcal{A}}_{R_{\widetilde{m}}}=h'_{R_{\widetilde{m}}D}\mathcal{M}\left(\widetilde{\mathbf{x}}_{R_{\widetilde{m}}}\right)$.

From (21), $\mathrm{APEP}\left(\mathbf{x}^{(D)}\rightarrow\widetilde{\mathbf{x}}^{(D)}\right)$ can be formulated as shown in (22), where (a) follows from the inverse Laplace transform with $\mathcal{P}$ being a small finite constant that lies in the region of convergence [44, Sec. 9B.2], [47, Sec. 2], and $\Phi_\Delta\left(\cdot|\cdot\right)$ is the moment generating function (MGF) of $\Delta\left(\cdot,\cdot|\cdot,\cdot\right)$, and can be formulated as shown in (23). In (23), (b) follows by using the identity $\mathbb{E}_{n_{RD}}\left\{\exp\left(-\mathrm{Re}\left\{zn_{RD}^*\right\}\right)\right\}=\exp\left(\left|z\right|^2\Big/4\right)$ for any complex number z [47, Eq. (19)].

From (23), $\Phi_\Delta\left(s\right)=\mathbb{E}_{\mathbf{h}_{RD}}\left\{\Phi_\Delta\left(s|\mathbf{h}_{RD}\right)\right\}$ can be formulated as follows:

$$\Phi_\Delta\left(s\right)\overset{(a)}{\approx}\begin{cases}\frac{1}{2}\left(\frac{\mathcal{F}_R(\widetilde{m})s(1-s)}{N_0}\right)^{-\frac{1}{2}}\left(\frac{-\mathcal{F}_R(m)s(1+s)}{N_0}\right)^{-\frac{1}{2}} & \text{if}\quad(\mathcal{C}1)\\ \left(\frac{\mathcal{F}_R(\widetilde{m})s(1-s)}{N_0}\right)^{-1} & \text{if}\quad(\mathcal{C}2)\\ \left(-\frac{\mathcal{F}_R(\widetilde{m})s(1+s)}{N_0}\right)^{-1} & \text{if}\quad(\mathcal{C}3)\end{cases}\tag{24}$$

where: i) $(\mathcal{C}1)$, $(\mathcal{C}2)$ and $(\mathcal{C}3)$ denote the cases $\sum\limits_{r\in\Omega_R^{(\mathrm{ON})}\left(\mathbf{x}^{(D)}\right)}\mathcal{A}_{R_r}\neq\widetilde{\mathcal{A}}_{R_{\widetilde{m}}}$ and $\sum\limits_{r\in\Omega_R^{(\mathrm{ON})}\left(\mathbf{x}^{(D)}\right)}A_{R_r}\neq A_{R_m}$, $\sum\limits_{r\in\Omega_R^{(\mathrm{ON})}\left(\mathbf{x}^{(D)}\right)}\mathcal{A}_{R_r}\neq\widetilde{\mathcal{A}}_{R_{\widetilde{m}}}$ and $\sum\limits_{r\in\Omega_R^{(\mathrm{ON})}\left(\mathbf{x}^{(D)}\right)}\mathcal{A}_{R_r}=\mathcal{A}_{R_m}$, and $\sum\limits_{r\in\Omega_R^{(\mathrm{ON})}\left(\mathbf{x}^{(D)}\right)}\mathcal{A}_{R_r}=\widetilde{\mathcal{A}}_{R_{\widetilde{m}}}$ and $\sum\limits_{r\in\Omega_R^{(\mathrm{ON})}\left(\mathbf{x}^{(D)}\right)}\mathcal{A}_{R_r}\neq\mathcal{A}_{R_m}$, respectively; and ii) (a) follows from Appendix I with $\mathcal{F}_R\left(\widetilde{m}\right)$ defined as shown in (25). Note that $\mathcal{F}_R\left(m\right)$ can be formulated similar to (25).

The expectation with respect to $\mathbf{h}_{SR}$ of $\Pr\left\{\mathbf{x}^{(D)}|\mathbf{h}_{RD}\right\}$ in (24) can be formulated as shown in (26), where: i)

$$\begin{aligned}\mathrm{PEP}\left(\mathbf{x}^{(D)}\rightarrow\widetilde{\mathbf{x}}^{(D)}|n_{RD},\mathbf{h}_{SR},\mathbf{h}_{RD}\right)&=\Pr\left\{\Lambda\left(\widetilde{\mathbf{x}}^{(D)}\right)-\Lambda\left(\mathbf{x}^{(D)}\right)<0|n_{RD},\mathbf{h}_{RD}\right\}\times\Pr\left\{\mathbf{x}^{(D)}|\mathbf{h}_{SR}\right\}\\&=\sum_{l_1=0}^{L+1}...\sum_{l_M=0}^{L+1}\left[\Pr\left\{\Delta\left(\mathbf{x}^{(D)},\widetilde{\mathbf{x}}^{(D)}\right)<0|n_{RD},\mathbf{h}_{RD}\right\}\Pr\left\{\mathbf{x}^{(D)}|\mathbf{h}_{RD}\right\}\right]\prod_{r\in\Omega_R}\Psi_{R_r}^{(l_r)}\end{aligned}\tag{20}$$

$$\mathrm{APEP}\left(\mathbf{x}^{(D)}\rightarrow\widetilde{\mathbf{x}}^{(D)}\right)\overset{(a)}{=}\sum_{l_1=0}^{L+1}...\sum_{l_M=0}^{L+1}\left[\frac{1}{2\pi j}\int_{\mathcal{P}-j\infty}^{\mathcal{P}+j\infty}\mathbb{E}_{\mathbf{h}_{RD}}\left\{\Phi_\Delta\left(s|\mathbf{h}_{RD}\right)\right\}\mathbb{E}_{\mathbf{h}_{SR}}\left\{\Pr\left\{\mathbf{x}^{(D)}|\mathbf{h}_{RD}\right\}\right\}\frac{ds}{s}\right]\prod_{r\in\Omega_R}\Psi_{R_r}^{(l_r)}\tag{22}$$

$$\begin{aligned}&\Phi_\Delta\left(s|\mathbf{h}_{RD}\right)=\mathbb{E}_{n_{RD}}\left\{-s\Delta\left(\mathbf{x}^{(D)},\widetilde{\mathbf{x}}^{(D)}|n_{RD},\mathbf{h}_{RD}\right)\right\}\\&\overset{(b)}{=}\exp\left(-\frac{\left|\sum\limits_{r\in\Omega_R^{(\mathrm{ON})}\left(\mathbf{x}^{(D)}\right)}\sqrt{E_R}\mathcal{A}_{R_r}-\sqrt{E_R}\widetilde{\mathcal{A}}_{R_{\widetilde{m}}}\right|^2}{N_0}s\left(1-s\right)\right)\times\exp\left(\frac{\left|\sum\limits_{r\in\Omega_R^{(\mathrm{ON})}\left(\mathbf{x}^{(D)}\right)}\sqrt{E_R}\mathcal{A}_{R_r}-\sqrt{E_R}\mathcal{A}_{R_m}\right|^2}{N_0}s\left(1+s\right)\right)\end{aligned}\tag{23}$$

$\omega_R^{(\mathrm{ON})}\left(\mathbf{x}^{(D)}\right)$ and $\mathcal{K}_R\left(\mathbf{x}^{(D)}\right)$ can be formulated similar to Section V-A; ii) (a) follows by applying the high-SNR approximation $1-Q\left(\sqrt{(E_S/N_0)\,x}\right)\approx 1$; iii) (b) follows by applying Chernoff bound and by noting that $|h'_{SR_r}|^2$ is an exponential RV. It is also worth noting that $\Omega_{R,\mathrm{neq}}^{(\mathrm{ON})}\left(\mathbf{x}^{(D)}\right)$ and $\Omega_{R,\mathrm{eq}}^{(\mathrm{OFF})}\left(\mathbf{x}^{(D)}\right)$ are disjoint sets. Therefore, the corresponding channels in these sets are statistically independent.

By inserting (24) and (26) in (22), we arrive at the expression for $\mathrm{APEP}\left(\mathbf{x}^{(D)}\to\widetilde{\mathbf{x}}^{(D)}\right)$ which is independent of instantaneous channel gains. The complex integral in (22) can be solved by using Gauss-Chebyshev quadrature rule as formulated in (27) [47, Eq. 10], shown at the bottom of this page. The integration pole $\mathcal{P}$, in accordance with [44, Sec. 9B.2], is set equal to one-half of the smallest real part of the non-negative poles of the MGF $\Phi_\Delta(s)$. Based on this consideration and by direct inspection of (24), $\mathcal{P}$ is chosen as follows:

$$\mathcal{P}=\begin{cases}1/2 & \text{if}\quad (\mathcal{C}1)\\ 1/2 & \text{if}\quad (\mathcal{C}2)\\ \text{does not exist} & \text{if}\quad (\mathcal{C}3)\end{cases} \tag{28}$$

The APEP contributes to the ASEP only if the poles exist. Therefore, during the computation of ASEP, the APEP pertaining to the case $(\mathcal{C}3)$ can be completely neglected. Finally, by using the union-bound method, the ASEP of the source in ER-DSM can be formulated as follows:

$$\mathrm{ASEP}\approx\sum_{\mathbf{x}^{(D)}}\sum_{\widetilde{\mathbf{x}}^{(D)}}\delta\left(\mathbf{x}_S^{(D)},\widetilde{\mathbf{x}}_S^{(D)}\right)\mathrm{APEP}\left(\mathbf{x}^{(D)}\to\widetilde{\mathbf{x}}^{(D)}\right) \tag{29}$$

B. Choice of $\alpha^{(\mathrm{ER})}$

From (22) and (26), it can be observed that the choice of $\alpha^{(\mathrm{ER})}$ effects the performance of ASEP in (29). Based on this consideration, we find the value of $\alpha^{(\mathrm{ER})}$ which provides the best error rate performance for ER-DSM.

The optimal value of $\alpha^{(\mathrm{ER})}$, denoted as $\alpha_*^{(\mathrm{ER})}$, can be obtained by solving the following optimization problem:

$$\begin{aligned}&\alpha_*^{(\mathrm{ER})}=\arg\min_{\alpha^{(\mathrm{ER})}}\left\{\mathrm{ASEP}\left(\alpha^{(\mathrm{ER})}\right)\right\}\\ &\text{subject}\quad\text{to}\quad 0<\alpha^{(\mathrm{ER})}<1\end{aligned} \tag{30}$$

Our simulations show that $\mathrm{ASEP}\left(\alpha^{(\mathrm{ER})}\right)$ has a unique global minimum point. However, it is difficult to find a closed-form solution due to the complexity of the expressions involved in the computation of $\mathrm{ASEP}\left(\alpha^{(\mathrm{ER})}\right)$, *i.e.*, (22)–(29). Therefore, in this paper, we resort to an exhaustive search method to find the optimal value of $\alpha^{(\mathrm{ER})}$ for a given system setup. We note here that a similar approach to finding the optimal solution has also been adopted in [8], where closed-form solutions were shown not to be available. It is also worth noting that the optimization in (30) is done from a system-level perspective and not from a link-level perspective. In other words, $\alpha_*^{(\mathrm{ER})}$ is chosen to obtain the best *average* performance of the system.

VII. Analytical and Simulation Results

In this section, we present analytical and simulation results for assessing the performance of ER-DSM, to substantiate the accuracy of our mathematical framework, and in order to

$$\mathcal{F}_R(\widetilde{m})=\sum_{r\in\Omega_R^{(\mathrm{ON})}\left(\mathbf{x}^{(D)}\right)}\frac{E_R}{L_{R_rD}}+\frac{E_R}{L_{R_{\widetilde{m}}D}}-\frac{2\mathbb{1}_{\Omega_R^{(\mathrm{ON})}\left(\mathbf{x}^{(D)}\right)}(\widetilde{m})\,E_R\,|\mathcal{M}(\mathbf{x}_{R_{\widetilde{m}}})|\,|\mathcal{M}(\widetilde{\mathbf{x}}_{R_{\widetilde{m}}})|}{L_{R_{\widetilde{m}}D}} \tag{25}$$

$$\begin{aligned}\mathbb{E}_{\mathbf{h}_{SR}}\left\{\Pr\left\{\mathbf{x}^{(D)}|\mathbf{h}_{SR}\right\}\right\}&\overset{(a)}{\approx}\left(\frac{1}{M}\right)\left(\frac{1}{N}\right)^{\omega_R^{(\mathrm{ON})}\left(\mathbf{x}^{(D)}\right)}\times\prod_{r\in\Omega_{R,\mathrm{neq}}^{(\mathrm{ON})}\left(\mathbf{x}^{(D)}\right)}\mathbb{E}_{\mathbf{h}_{SR}}\left\{Q\left(\sqrt{\frac{\left(1-\alpha^{(\mathrm{ER})}\right)E_S}{2N_0}|d_S(\mathbf{ID}_{R_r})|^2|h'_{SR_r}|^2}\right)\right\}\\&\times\prod_{r\in\Omega_{R,\mathrm{eq}}^{(\mathrm{OFF})}\left(\mathbf{x}^{(D)}\right)}\mathbb{E}_{\mathbf{h}_{SR}}\left\{\beta_aQ\left(\sqrt{2\beta_b\frac{\left(1-\alpha^{(\mathrm{ER})}\right)E_S}{N_0}|h'_{SR_r}|^2}\right)\right\}\\&\overset{(b)}{\approx}\mathcal{K}_R\left(\mathbf{x}^{(D)}\right)\left(\frac{1}{M}\right)\times\prod_{r\in\Omega_{R,\mathrm{neq}}^{(\mathrm{ON})}\left(\mathbf{x}^{(D)}\right)}(\Upsilon_{R_r})^{-\delta\left(|d_S(\mathbf{ID}_{R_r})|^2,0\right)}\times\prod_{r\in\Omega_{R,\mathrm{eq}}^{(\mathrm{OFF})}\left(\mathbf{x}^{(D)}\right)}(\xi_{R_r})^{-1}\end{aligned} \tag{26}$$

$$\begin{aligned}\overline{\Phi}_\Delta(s)&=\frac{1}{2\pi j}\int_{\mathcal{P}-j\infty}^{\mathcal{P}+j\infty}\Phi_\Delta(s)\frac{ds}{s}\\&=\frac{1}{2\pi}\int_{-1}^{+}\frac{1}{\sqrt{1-x^2}}\mathrm{Re}\left\{\Phi_\Delta\left(\mathcal{P}+j\mathcal{P}\frac{\sqrt{1-x^2}}{x}\right)\right\}dx+\frac{1}{2\pi}\int_{-1}^{+}\frac{1}{x}\mathrm{Im}\left\{\Phi_\Delta\left(\mathcal{P}+j\mathcal{P}\frac{\sqrt{1-x^2}}{x}\right)\right\}dx\end{aligned} \tag{27}$$

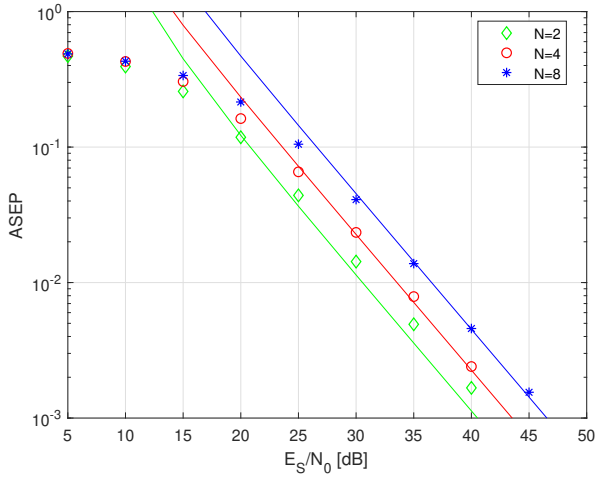

Fig. 6: Comparison of Monte Carlo simulations (markers) and the mathematical framework in Section VI (solid lines). Setup: $M = 2$, $\tau_R = 5$, $\kappa_R = 10$, $L = 200$ and $\mathcal{D}_{SR} = \mathcal{D}_{RD} = \mathcal{D}_{RR} = 2$m.

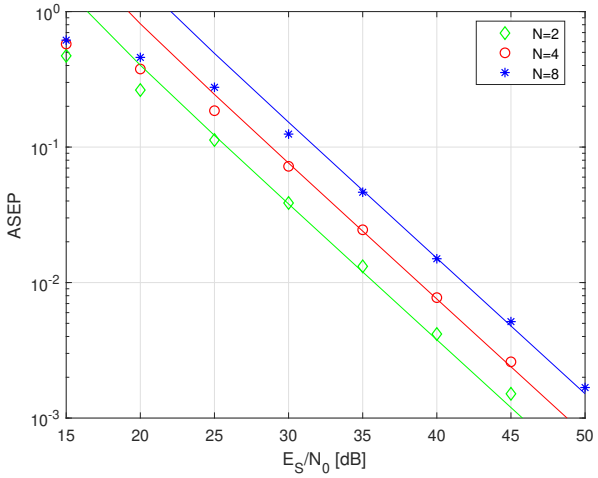

Fig. 7: Comparison of Monte Carlo simulations (markers) and the mathematical framework in Section VI (solid lines). Setup: $M = 4$, $\tau_R = 10$, $\kappa_R = 2$, $L = 100$ and $\mathcal{D}_{SR} = \mathcal{D}_{RD} = \mathcal{D}_{RR} = 2$m.

compare the performance of ER-DSM against PS-DSM and PS aided Demodulate-and-Forward (PS-DemF) protocol.

a) System Parameters: The proposed framework for the performance analysis of ER-DSM is general, and can account for various system parameters and network topologies. For illustrative purposes, however, we consider the following setups: i) the energy conversion efficiency, $\eta = 0.8$; ii) PSK modulation is employed at the source and the relays; iii) $N_c = -70$ dBm; iv) $f_{carr} = 800$ MHz; v) $G_X = G_Y = 15$ dB for all node pairs (X,Y); and vi) the battery of each relay is set to be empty before the beginning of the first transmission. Other parameters used to obtain the curves are provided in the caption of each figure. Also, for the ease of reproducibility of the figures, the optimal values of $\alpha^{(\mathrm{ER})}$, *i.e.*, $\alpha_*^{(\mathrm{ER})}$ is also provided in the caption of the corresponding figures. Furthermore, the optimal values for $\alpha_{R_r}^{(\mathrm{PS})}$ and $\alpha^{(\mathrm{PS-DemF})}$, denoted as $\alpha_{*R_r}^{(\mathrm{PS})}$ and $\alpha_*^{(\mathrm{PS-DemF})}$, respectively, are also provided in the caption of the figures. The values of $\alpha_{*R_r}^{(\mathrm{PS})}$ and $\alpha_*^{(\mathrm{PS-DemF})}$ are obtained by using exhaustive search.

b) Validation of the analytical framework: In Fig. 6 and Fig 7, the accuracy of the analytical framework in Section VI (and Section V) is compared against Monte Carlo simulations for various network topologies, modulation orders and transmit powers at the source/relays, battery sizes and battery levels. We observe that a good accuracy is obtained, in particular in the high-SNR regime, for the analysed system setups. Furthermore, these results also mostly validate the approximations used to obtain the analytical steady-state distribution[12] and the ASEP. In fact, the approximations were essential to obtaining a relatively simple closed-form expression for the ASEP. We note here that due to the nature of the applied approximations/bounds, the analytical ASEP does not constitute either an upper-bound or a lower-bound, and is in fact, only an approximation. We further note that, although the analytical framework developed in this paper is tight for many system setups, the framework will not be tight in scenarios where the approximation in Remark 2 is loose. The framework that encompasses such scenarios may be mathematically complex to develop, however, the mathematical development used in this paper may serve as a reference.

[12]Recall that the analytical framework for the steady-state distribution is compared against Monte Carlo simulations in Fig. 5 of Section V.

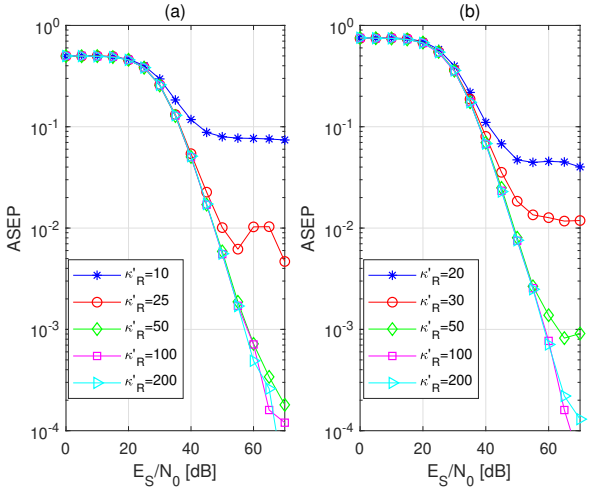

Fig. 8: The performance of ER-DSM for different battery sizes. Setup: (a) $M = 2$, $N = 2$, $\tau_R = 5$, $L = 500$ and $\mathcal{D}_{SR} = \mathcal{D}_{RD} = \mathcal{D}_{RR} = 2$m. (b) $M = 4$, $N = 2$, $\tau_R = 10$, $L = 500$ and $\mathcal{D}_{SR} = \mathcal{D}_{RD} = \mathcal{D}_{RR} = 2$m. Only Monte carlo simulation results are shown. In (a), the values of $\alpha_*^{(\mathrm{ER})}$ are 0.75, 0.85, 0.70, 0.35 and 0.85 for $\kappa'_R = 10, 25, 50, 100$ and 200, respectively. In (b), the values of $\alpha_*^{(\mathrm{ER})}$ are 0.90, 0.80, 0.75, 0.40 and 0.60 for $\kappa'_R = 20, 30, 50, 100$ and 200, respectively.

c) Impact of the size of the battery: In Fig. 8a and Fig. 8b, we analyse the impact of the battery storage size on the performance of ER-DSM. The increase in storage size is captured by the battery scaling factor κ'_R, with $E_{\max} = \mathcal{E}'^{(\kappa'_R)}$ and $\mathcal{E}'^{(i)} = iE_S/(L+1)$. Furthermore, $E_R = \mathcal{E}'^{(\tau_R)}$. These slight changes in formulations decouple $E_{\max}$ and E_R, and focus only the influence of $E_{\max}$ on the system performance. We observe that as κ'_R is increased from 2 to 100, ASEP

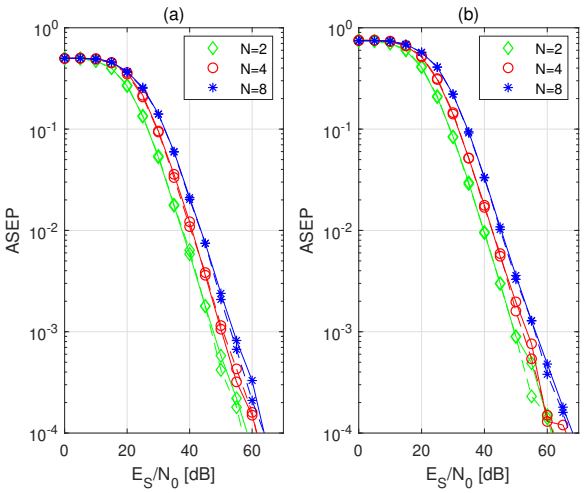

Fig. 9: The performance comparison of ER-DSM (solid lines) and PS-DSM (dashed lines). Setup: (a) $M = 2$, $\kappa_R = 10$, $\tau_R = 5$, $L = 500$ and $\mathcal{D}_{SR} = \mathcal{D}_{RD} = \mathcal{D}_{RR} = 2$m. (b) $M = 4$, $\kappa_R = 20$, $\tau_R = 5$, $L = 500$ and $\mathcal{D}_{SR} = \mathcal{D}_{RD} = \mathcal{D}_{RR} = 2$m. Only Monte carlo simulation results are shown. In (a), the values of $\alpha_*^{(\mathrm{ER})}$ and $\alpha_{*\,R_r}^{(\mathrm{PS})}$, respectively, are 0.70 and 0.70 ($N = 2$), 0.85 and 0.60 ($N = 4$), and 0.75 and 0.60 ($N = 8$). In (b), the values of $\alpha_*^{(\mathrm{ER})}$ and $\alpha_{*\,R_r}^{(\mathrm{PS})}$, respectively, are 0.40 and 0.50 ($N = 2$), 0.40 and 0.55 ($N = 4$), and 0.60 and 0.50 ($N = 8$).

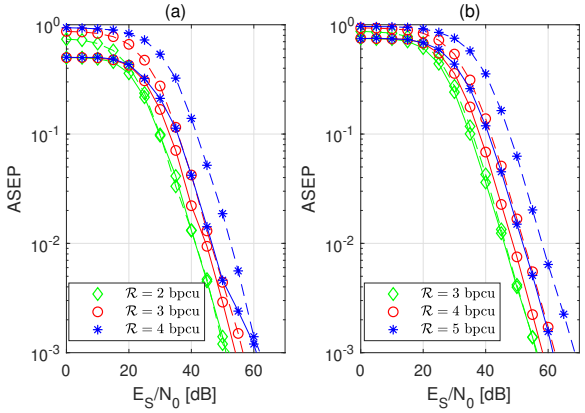

Fig. 10: The performance comparison of ER-DSM (solid lines) and PS-DemF (dashed lines). Setup: (a) $\mathcal{R} = 2$ bpcu: $M = 2$, $N = 2$ and $M' = 4$; $\mathcal{R} = 3$ bpcu: $M = 2$, $N = 4$ and $M' = 8$; and $\mathcal{R} = 4$ bpcu: $M = 2$, $N = 8$ and $M' = 16$. (b) $\mathcal{R} = 3$ bpcu: $M = 4$, $N = 2$ and $M' = 8$; $\mathcal{R} = 4$ bpcu: $M = 4$, $N = 4$ and $M' = 16$; and $\mathcal{R} = 5$ bpcu: $M = 4$, $N = 8$ and $M' = 32$. The values of $\alpha_*^{(\mathrm{PS-DemF})}$ are 0.05 ($\mathcal{R} = 2$), 0.35 ($\mathcal{R} = 3$), 0.30 ($\mathcal{R} = 4$), and 0.15 ($\mathcal{R} = 5$). In (a), the values of $\alpha_*^{(\mathrm{ER-DSM})}$ are 0.65 ($\mathcal{R} = 2$), 0.70 ($\mathcal{R} = 3$) and 0.30 ($\mathcal{R} = 4$). In (b), the values of $\alpha_*^{(\mathrm{ER-DSM})}$ are 0.45 ($\mathcal{R} = 3$), 0.55 ($\mathcal{R} = 4$) and 0.50 ($\mathcal{R} = 5$). The following parameters are considered to be the same in both (a) and (b): $\kappa_R = 2$, $\tau_R = 10$, $L = 500$ and $\mathcal{D}_{SR} = \mathcal{D}_{RD} = \mathcal{D}_{RR} = 2$m.

decreases (at high SNR values). This trend can be attributed to the reduction in energy loss due to energy overflow, which leads to a higher portion of energy being delegated for the information forwarding operation [17]. As the battery size is increased further, *i.e.*, for $\kappa_R' > 100$, the performance remains (almost) the same, as the energy overflow is less frequent when the battery size is sufficiently large.

d) Performance comparison of ER-DSM and PS-DSM: In Fig. 9, we compare the performance of ER-DSM against PS-DSM. More specifically, in Fig. 9a, we have used $\kappa_R = 10$ (for $M = 2$), and in Fig. 9b, $\kappa_R = 20$ (for $M = 4$) have been used. From Fig. 9, we also observe that the performance of ER-DSM and PS-DSM are almost the same for the analysed system setups. However, a notable advantage of ER-DSM over PS-DSM, as highlighted in *Remark 1*, is that ER-DSM does not require complicated power splitting circuitry, which increases the complexity and cost of the hardware, at the relays. Therefore, ER-DSM is relatively a low-complexity alternative to PS-DSM.

e) Performance comparison of ER-DSM and PS-DemF: In Fig. 10, the performance of ER-DSM is compared against PS-DemF for various system setups. In PS-DemF, we consider a source, a relay and a destination, each equipped with a single-antenna. During the first time-slot, the source transmits its data symbol to the relay. The power splitter at the relay splits the received signal in two parts (similar to PS-DSM) - one part for demodulation of the information, and the other for energy harvesting. The energy is harvested in a battery which has been modeled similar to Section II. The demodulated data is then forwarded to the destination during the next time-slot. The corresponding demodulation at the destination can be formulated similar to (5). It is also worth emphasizing here that the number of *active* relays in PS-DemF and ER-DSM (when there are no errors at the relays) is also the same at any given time-slot, however, ER-DSM requires a higher number of cooperating relays (all but one is inactive).

The average rate, $\mathcal{R}$, of ER-DSM is $\log_2(M) + \log_2(N)$ bpcu [1], and that of PS-DemF is $\log_2(M')$, with M' being the signal constellation size used at the source. Therefore, for ensuring a fair comparison, $\mathcal{R}$ for both ER-DSM and PS-DemF are forced to be the same. For the considered setup in Fig. 10, we observe that the performance of ER-DSM is slightly better than PS-DemF for higher data rates. However, their performances are almost the same in other instances. This behaviour, is in fact, similar to those observed for traditional (without SWIPT) DSM and DemF, as shown in [1]. We also note here that unlike PS-DemF, the relays in ER-DSM have their own data to transmit. In ER-DSM, the relays' jointly forward its own data and the source's data to the destination. In fact, as mentioned in Section I, the source's data is implicitly forwarded from the relays by using the SM principle. Therefore, the modulation domain is used exclusively for forwarding the relays' own data. The can translate to better coding gain for ER-DSM. Furthermore, the advantage in terms of ASEP becomes more pronounced when N, and consequently the overall data rate, becomes larger.

f) Impact of Relay Location: In Fig. 10, we show the performance of ER-DSM for different values of the source-to-relay distance, $\mathcal{D}_{SR}$. We have set both the relay-to-relay distance, $\mathcal{D}_{SR}$, and the relay-to-destination distance $\mathcal{D}_{RD}$ as equal to 2m. It can be observed that, as expected, as $\mathcal{D}_{SR}$ increases, ASEP correspondingly increases. This is because, as the path-loss increases, the received signal strength at the relays, which are utilized for powering the relays and decoding the information transmitted from the source, decreases. Consequently, this leads to reduced error performance at the destination for ER-DSM.

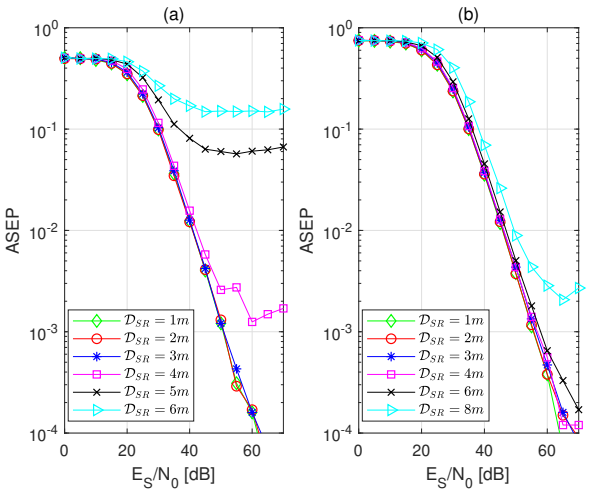

Fig. 11: Performance of ER-DSM for different values of source-to-relay distance, $\mathcal{D}_{SR}$. Setup: (a) $M = 2$, $N = 2$, $\tau_R = 10$, $\kappa_R = 2$ and $L = 500$. (b) $M = 4$, $N = 2$, $\tau_R = 10$, $\kappa_R = 2$ and $L = 500$. Only Monte Carlo simulation results are shown. In (a), the values of $\alpha_*{}^{(\mathrm{ER})}$ are 0.40 ($\mathcal{D}_{SR}$ = 1m), 0.30 ($\mathcal{D}_{SR}$ = 2m), 0.65 ($\mathcal{D}_{SR}$ = 3m), 0.80 ($\mathcal{D}_{SR}$ = 4m), 0.90 ($\mathcal{D}_{SR}$ = 5m) and 0.90 ($\mathcal{D}_{SR}$ = 6m). In (b), the values of $\alpha_*{}^{(\mathrm{ER})}$ are 0.50 ($\mathcal{D}_{SR}$ = 1m), 0.30 ($\mathcal{D}_{SR}$ = 2m), 0.45 ($\mathcal{D}_{SR}$ = 3m), 0.30 ($\mathcal{D}_{SR}$ = 4m), 0.50 ($\mathcal{D}_{SR}$ = 6m) and 0.75 ($\mathcal{D}_{SR}$ = 8m). In both (a) and (b), we have considered $\mathcal{D}_{RR} = \mathcal{D}_{RD} = 2$m.

VIII. Conclusion

In this paper, two protocols - PS-DSM and ER-DSM - have been introduced to enable DSM with SWIPT capability. The PS-DSM exploits power splitters at the relay nodes to harvest energy transmitted from the source, which is then used by the relay to forward its own data and the source's data, simultaneously. The ER-DSM, on the other hand, in addition to harvesting the energy transmitted from the source, also exploits the inactive cooperating relays to recycle part of the transmitted energy in the network. Furthermore, unlike PS-DSM, ER-DSM does not rely on power splitters (or time switches) at the relay nodes, and hence, the hardware complexity and cost is lower for ER-DSM. Due to its particular operating principle, we have analytically studied the performance of ER-DSM by first introducing a Markov chain formulation for modelling the charging/discharging behaviour of the relay batteries, and then utilising the proposed Markov chain model for obtaining a mathematical framework for computing the ASEP. Although not considered in this paper due to space limitation, the framework for PS-DSM can be developed similar to ER-DSM. The framework for ER-DSM has been substantiated with the aid of Monte Carlo simulations, and it has been shown to be sufficiently tight in the high-SNR regime for many system setups. A tighter framework for more general setups is currently under investigation. Finally, it has also been shown that ER-DSM is capable of outperforming, in terms of ASEP, PS-DSM and PS-DemF in certain scenarios.

Appendix I
Computation of $\Phi_\Delta(\cdot)$ in (24)

In order to compute the expectation of $\Phi_\Delta(s|\mathbf{h}_{RD})$ with respect to $\mathbf{h}_{RD}$ in (23), three cases have to be considered.

Case 1: $\sum_{r\in\Omega_R^{(\mathrm{ON})}(\mathbf{x}^{(D)})} \mathcal{A}_{R_r} \neq \widetilde{\mathcal{A}}_{R_{\widetilde{m}}}$ and $\sum_{r\in\Omega_R^{(\mathrm{ON})}(\mathbf{x}^{(D)})} \mathcal{A}_{R_r} \neq \mathcal{A}_{R_m}$: From (23), we have the expression for $\Phi_\Delta(s|\mathbf{h}_{RD})$ as the product of two exponential terms. By direct inspection of (23), it can be readily observed that $\sum_{r\in\Omega_R^{(\mathrm{ON})}(\mathbf{x}^{(D)})} \sqrt{E_R}\mathcal{A}_{R_r} - \sqrt{E_R}\widetilde{\mathcal{A}}_{R_{\widetilde{m}}}$ and $\sum_{r\in\Omega_R^{(\mathrm{ON})}(\mathbf{x}^{(D)})} \sqrt{E_R}A_{R_r} - \sqrt{E_R}A_{R_m}$ are not independent RVs, and hence, a closed form solution to the expectation of $\Phi_\Delta(s|\mathbf{h}_{RD})$ is difficult to derive. However, it can be solved by approximating (bounding) with the aid of Cauchy-Schwarz inequality [45]. Applying Cauchy-Schwarz inequality to (23), we obtain:

$$\Phi_\Delta(s) = \mathbb{E}_{\mathbf{h}_{RD}}\{\Phi_\Delta(s|\mathbf{h}_{RD})\} \leq \sqrt{\mathcal{C}_1 \times \mathcal{C}_2} \tag{31}$$

where $\mathcal{C}_1$ and $\mathcal{C}_2$ are defined as shown in (32) and (33), respectively, where $(a1)$ and $(a2)$ follow after some algebra, noting that the RVs follow an exponential distribution with $\mathcal{F}_R(\cdot)$ defined in (25), and $(b1)$ and $(b2)$ hold in the high-SNR regime.

Case 2: $\sum_{r\in\Omega_R^{(\mathrm{ON})}(\mathbf{x}^{(D)})} \mathcal{A}_{R_r} \neq \widetilde{\mathcal{A}}_{R_{\widetilde{m}}}$ and $\sum_{r\in\Omega_R^{(\mathrm{ON})}(\mathbf{x}^{(D)})} \mathcal{A}_{R_r} = \mathcal{A}_{R_m}$: Accordingly, we have:

$$\Phi_\Delta(s) \approx \left(\frac{\mathcal{F}_R(\widetilde{m})\, s\,(1-s)}{N_0}\right)^{-1} \tag{34}$$

Case 3: $\sum_{r\in\Omega_R^{(\mathrm{ON})}(\mathbf{x}^{(D)})} \mathcal{A}_{R_r} = \widetilde{\mathcal{A}}_{R_{\widetilde{m}}}$ and $\sum_{r\in\Omega_R^{(\mathrm{ON})}(\mathbf{x}^{(D)})} \mathcal{A}_{R_r} \neq \mathcal{A}_{R_m}$: Accordingly, we have:

$$\Phi_\Delta(s) \approx \left(-\frac{\mathcal{F}_R(\widetilde{m})\, s\,(1+s)}{N_0}\right)^{-1} \tag{35}$$

It is worth noting that, from the definition of PEP, $x_S^{(D)} \neq \widetilde{x}_S^{(D)}$, *i.e.*, $m \neq \widetilde{m}$. Therefore, the scenario $\sum_{r\in\Omega_R^{(\mathrm{ON})}(\mathbf{x}^{(D)})} \mathcal{A}_{R_r} = \widetilde{\mathcal{A}}_{R_{\widetilde{m}}}$ and $\sum_{r\in\Omega_R^{(\mathrm{ON})}(\mathbf{x}^{(D)})} \mathcal{A}_{R_r} = \mathcal{A}_{R_m}$ cannot exist simultaneously. Finally, the expression for $\Phi_\Delta(s)$ in (24) follows with the aid of (31) –(35). This concludes the proof.

References

[1] S. Narayanan, M. Di Renzo, F. Graziosi, and H. Haas, "Distributed Spatial Modulation: A Cooperative Diversity Protocol for Half-Duplex Relay-Aided Wireless Networks", *IEEE Trans. Veh. Technol.*, vol. 65, no. 5, pp. 2947-2964, May 2016.

[2] S. Bi, C. K. Ho, and R. Zhang, "Wireless powered communication: Opportunities and challenges", *IEEE Commun. Mag.*, vol. 53, no. 4. pp.117-125, Apr. 2015.

[3] I. Krikidis, S. Timotheou, S. Nikolaou, G. Zheng, D. W. K. Ng, and R. Schober, "Simultaneous wireless information and power transfer in modern communication systems", *IEEE Commun. Mag.*, vol. 52, no. 11, pp. 104-110, Nov. 2014.

[4] M. Naslcheraghi, S. A. Ghorashi, and M. Shikh-Bahaei, "FD device-to-device communication for wireless video distribution", *IET Commun.*, vol. 11, no. 7, pp. 1074-1081, May 2017.

[5] R. Zhang and C. K. Ho, "MIMO broadcast for simultaneous wireless information and power transfer", *IEEE Trans. Wireless Commun.*, vol. 12, no. 5, pp. 1989-2001, May 2013.

[6] J. Park and B. Clerckx, "Joint Wireless Information and Energy Transfer in a Two-User MIMO Interference Channel", *IEEE Trans. Wireless Comm.*, vol. 12, no. 8, 2013, pp. 4210-4221.

[7] T. Tu Lam, M. Di Renzo and J. P. Coon, "System-Level Analysis of SWIPT MIMO Cellular Networks", *IEEE Commun. Lett.*, vol. 20, no. 10, pp. 2011-2014, Oct. 2016.

[8] A. A. Nasir, X. Zhou, S. Durrani, and R. A. Kennedy, "Relaying protocols for wireless energy harvesting and information processing", *IEEE Trans. Wireless Commun.*, vol. 12, no. 7, pp. 3622-3636, Jul. 2013.

[9] I. Krikidis, S. Sasaki, S. Timotheou, and Z. Ding, "A low complexity antenna switching for joint wireless information and energy transfer in MIMO relay channels", *IEEE Trans. Commun.*, vol. 62, no. 5, pp. 1577-1587, May 2014.

[10] I. Krikidis, "Simultaneous information and energy transfer in large-scale networks with/without relaying", *IEEE Trans. Commun.*, vol. 62, no. 3, pp. 900-912, Mar. 2014.

[11] D. Wang, R. Zhang, X. Cheng, L. Yang and C. Chen, "Relay Selection in Full-Duplex Energy-Harvesting Two-Way Relay Networks", *IEEE Trans. Green Commun. and Netw.*, vol. 1, no. 2, pp. 182-191, June 2017.

[12] D. Wang, R. Zhang, X. Cheng and L. Yang, "Capacity-Enhancing Full-Duplex Relay Networks based on Power-Splitting (PS-)SWIPT", *IEEE Trans. Veh. Technol.*, vol. 66, no. 6, pp. 5445-5450, June 2017.

[13] Y. Zeng and R. Zhang, "Full-duplex wireless-powered relay with self-energy recycling", *IEEE Wireless Commun. Lett.*, vol. 4, no. 2, pp. 201-204, Apr. 2015.

[14] I. Krikidis, "Relay Selection in Wireless Powered Cooperative Networks With Energy Storage", *IEEE Journal on Selected Areas in Commun.*, vol. 33, no. 12, pp. 2596-2610, Dec. 2015.

[15] I. Krikidis, S. Timotheou, and S. Sasaki, "RF energy transfer for cooperative networks: Data relaying or energy harvesting?", *IEEE Commun. Lett.*, vol. 16, no. 11, pp. 1772-1775, Nov. 2012.

[16] K. H. Liu, "Performance Analysis of Relay Selection for Cooperative Relays Based on Wireless Power Transfer With Finite Energy Storage", *IEEE Trans. Veh. Technol.*, vol. 65, no. 7, pp. 5110-5121, July 2016.

[17] Y. Gu, H. H. Chen, Y. Li and B. Vucetic, "Distributed multi-relay selection in wireless-powered cooperative networks with energy accumulation", *IEEE Int. Conf. Commun.*, pp. 1-6., Sept. 2016.

[18] X. Lu, P. Wang, D. Niyato, D. I. Kim, and Z. Han, "Wireless networks with RF energy harvesting: A contemporary survey", *IEEE Commun. Surveys Tuts.*, vol. 17, no. 2, pp. 757-789, Second Quart. 2015.

[19] R. Y. Mesleh *et. al.*, "Spatial modulation", *IEEE Trans. Veh. Technol.*, vol. 57, no. 4, pp. 2228-2241, July 2008.

[20] *NetWorld2020–European Technology Platform for Communications Network and Services*, *White Paper Res. Beyond 5G*, Feb. 2016.

[21] M. Di Renzo and H. Haas, "Bit error probability of SM-MIMO over generalized fading channels", *IEEE Trans. Veh. Technol.*, vol. 61, no. 3, pp. 1124-1144, Mar. 2012.

[22] M. Di Renzo and H. Haas, "On transmit-diversity for spatial modulation MIMO: Impact of spatial constellation diagram and shaping filters at the transmitter", *IEEE Trans. Veh. Technol.*, vol. 62, no. 6, pp. 2507-2531, July 2013.

[23] Y. Bian *et.al.*, "Differential Spatial Modulation", *IEEE Trans. Veh. Technol.*, vol. 64, no. 7, pp. 3262-3268, July 2015.

[24] A. Stavridis, S. Sinanovic, M. Di Renzo, H. Haas, and P. M. Grant, "An energy saving base station employing spatial modulation," *IEEE Int. Workshop Comput.-Aided Model. Anal. Des. Commun. Links Netw.*, pp. 1-6, Sep. 2012.

[25] G. Zafari, M. Koca and H. Sari, "Dual-Polarized Spatial Modulation Over Correlated Fading Channels", *IEEE Trans. Commun.*, vol. 65, no. 3, pp. 1336-1352, Mar. 2017.

[26] S. Narayanan, M. Di Renzo, M. J. Chaudhry, F. Graziosi, and H. Haas, "On the Achievable Performance-Complexity Tradeoffs of Relay-Aided Space Shift Keying", *IEEE Trans. Signal and Inf. Processing Over Networks*, vol. 1, no. 2, pp. 129-144, June 2015.

[27] Y. Yang, "Information-guided relay selection for high throughput in half-duplex relay channels", *IEEE Global Commun. Conf.*, Nov./Dec. 2009, pp. 1–5.

[28] P. Yang, B. Zhang, Y. Xiao, B. Dong, S. Li, M. El–Hajjar, and L. Hanzo, "Detect–and–forward relaying aided cooperative spatial modulation for wireless networks", *IEEE Trans. Commun.*, vol. 61, no. 11, pp. 4500-4511, Nov. 2013.

[29] S. Narayanan, M. Di Renzo, F. Graziosi, and H. Haas, "Distributed Spatial Modulation for Relay Networks", *IEEE Veh. Technol. Conf.-Fall*, pp. 1-6, Sep. 2013.

[30] P. Patcharamaneepakorn *et.al.*, "Spectral, Energy and Economic Efficiency of 5G Multi-cell Massive MIMO Systems with Generalized Spatial Modulation", *IEEE Trans. Veh. Technol.*, vol. 65, no. 12, pp. 9715-9731, Dec. 2016.

[31] T. Lakshmi Narasimhan, P. Raviteja and A. Chockalingam, "Generalized Spatial Modulation in Large-Scale Multiuser MIMO Systems", *IEEE Trans. Wireless Commun.*, vol. 14, no. 7, pp. 3764-3779, July 2015.

[32] B. Jiao *et. al.*, "Spatial Modulated Full Duplex", *IEEE Wireless Commun. Lett.*, vol. 3, no. 6, pp. 641-644, Dec. 2014.

[33] J. Zhang, Q. Li, K. Kim, Y. Wang, X. Ge, J. Zhang, "On the Performance

$$\mathcal{C}_1 = \mathbb{E}_{\mathbf{h}_{RD}} \left\{ \exp\left(-2 \frac{\left| \sum\limits_{r \in \Omega_R^{(\mathrm{ON})}\left(\mathbf{x}^{(D)}\right)} \sqrt{E_{R_r}} \mathcal{A}_{R_r} - \sqrt{E_R} \widetilde{\mathcal{A}}_{R_{\widetilde{m}}} \right|^2}{N_0} s\left(1-s\right) \right) \right\} \tag{32}$$
$$\overset{(a1)}{=} \left(1 + \frac{2\mathcal{F}_R\left(\widetilde{m}\right) s\left(1-s\right)}{N_0} \right)^{-1} \overset{(b1)}{\approx} \left(\frac{2\mathcal{F}_R\left(\widetilde{m}\right) s\left(1-s\right)}{N_0} \right)^{-1}$$

$$\mathcal{C}_2 = \mathbb{E}_{\mathbf{h}_{RD}} \left\{ \exp\left(2 \frac{\left| \sum\limits_{r \in \Omega_R^{(\mathrm{ON})}\left(\mathbf{x}^{(D)}\right)} \sqrt{E_{R_r}} \mathcal{A}_{R_r} - \sqrt{E_R} \mathcal{A}_{R_m} \right|^2}{N_0} s\left(1+s\right) \right) \right\} \tag{33}$$
$$\overset{(a2)}{=} \left(1 - \frac{2\mathcal{F}_R\left(m\right) s\left(1+s\right)}{N_0} \right)^{-1} \overset{(b2)}{\approx} \left(-\frac{2\mathcal{F}_R\left(m\right) s\left(1+s\right)}{N_0} \right)^{-1}$$

of Full-duplex Two-way Relay Channels with Spatial Modulation", *IEEE Trans. Commun.*, vol. 64, no. 12, pp. 4966-4982, Dec. 2016.
[34] N. Ishikawa, R. Rajashekar, S. Sugiura and L. Hanzo, "Generalized Spatial Modulation Based Reduced-RF-Chain Millimeter-Wave Communications", *IEEE Trans. Veh. Technol.*, vol. 66, no. 1, pp. 879-883, Jan. 2017.
[35] N. S. Perović, P. Liu, M. Di Renzo and A. Springer, "Receive Spatial Modulation for LOS mmWave Communications Based on TX Beamforming", *IEEE Commun. Lett.*, vol. 21, no. 4, pp. 921-924, April 2017.
[36] S. Guo, H. Zhang, Y. Wang and D. Yuan, "Spatial Modulated Simultaneous Wireless Information and Power Transfer", *IEEE Global Commun. Conf.*, Dec. 2016, pp. 1-6.
[37] M. Zhang; X. Cheng, "Spatial-Modulation Based Wireless-Powered Communication for Achievable Rate Enhancement", *IEEE Commun. Lett.*, vol. 21, no. 6, pp. 1365-1368, June 2017.
[38] M. Di Renzo, H. Haas, A. Ghrayeb, S. Sugiura, and L. Hanzo, "Spatial modulation for generalized MIMO: Challenges, opportunities and implementation", *Proc. of the IEEE*, vol. 102, no. 1, pp. 56-103, Jan. 2014.
[39] Y. Gu and S. Aïssa, "RF-Based Energy Harvesting in Decode-and-Forward Relaying Systems: Ergodic and Outage Capacities", *IEEE Trans. Wireless Commun.*, vol. 14, no. 11, pp. 6425-6434, Nov. 2015.
[40] E. G. Larsson and B. R. Vojcic, "Cooperative transmit diversity based on superposition modulation", *IEEE Commun. Lett.*, vol. 9, vol. 9, pp. 778-780, Sep. 2005.
[41] X. Zhou, R. Zhang and C. K. Ho, "Wireless Information and Power Transfer: Architecture Design and Rate-Energy Tradeoff", *IEEE Trans. Commun.*, vol. 61, no. 11, pp. 4754-4767, Nov. 2013.
[42] S. Haykins, *Communication systems*, Wiley, 2001.
[43] X. Di, K. Xiong, P. Fan and H. C. Yang, "Simultaneous Wireless Information and Power Transfer in Cooperative Relay Networks With Rateless Codes", *IEEE Trans. Veh. Technol.*, vol. 66, no. 4, pp. 2981-2996, Apr. 2017.
[44] M. K. Simon and M.-S. Alouini, *Digital Communication over Fading Channels*, John Wiley & Sons, 2nd ed., 2005.
[45] M. Haenggi, *Stochastic Geometry for Wireless Networks*. Cambridge, U.K.: Cambridge Univ. Press, 2013.
[46] J. R. Norris, *Markov Chains*. Cambridge University Press, 1998.
[47] E. Biglieri, C. Caire, G. Taricco, and J. Ventura-Traveset, "Computing error probabilities over fading channels: A unified approach", *European Trans. Telecommun.*, vol. 9, no. 1, pp. 15-25, Feb. 1998.
[48] K. Nehra, A. Shadmand and M. Shikh-Bahaei, "Cross-Layer Design for Interference-Limited Spectrum Sharing Systems", *IEEE Global Commun. Conf.* pp. 1-5, Dec. 2010.
[49] A. Kobravi and M. Shikh-Bahaei,, "Cross-Layer Adaptive ARQ and Modulation Tradeoffs", *IEEE Int. Sym. Pers. Indoor and Mobile Radio Commun.* pp. 1-5, 2007.
[50] K. Nehra and M. Shikh-Bahaei, "Spectral Efficiency of Adaptive MQAM/OFDM Systems With CFO Over Fading Channels", *IEEE Trans. Veh. Technol.*, vol. 60, no. 3, pp. 1240-1247, Mar. 2011.

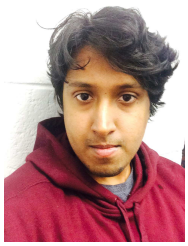

Sandeep Narayanan (M'16) received the B.Tech. degree from Amrita University, India, in 2010, the M.Sc. degree from The University of Edinburgh, U.K., in 2011, and the Ph.D. degree in electrical and information engineering from the University of L'Aquila, Italy, in 2015. From 2011 to 2014, he was a Marie-Curie Early Stage Researcher with the Center of Excellence for Research DEWS, University of L'Aquila, and Wireless Embedded Systems Technologies Aquila, Italy. He was a Post-Doctoral Research Fellow with University College Dublin, Ireland, and a Research Associate with the Centre for Telecommunications Research, King's College London, UK. He has also held visiting research positions at Northwestern University, USA, and The University of Edinburgh. His main research interests include wireless communication theory and signal processing.

Mohammad Shikh-Bahaei (S'96–M'00–SM'08) received the B.Sc. degree from the University of Tehran, Tehran, Iran, in 1992, the M.Sc. degree from the Sharif University of Technology, Tehran, Iran, in 1994, and the Ph.D. degree from King's College London, U.K., in 2000. He has worked for two start-up companies, and for National Semiconductor Corp., Santa Clara, CA, USA (now part of Texas Instruments Incorporated), on the design of third-generation (3G) mobile handsets, for which he has been awarded three U.S. patents as inventor and co-inventor, respectively. In 2002, he joined King's College London as Lecturer, where he is now a full Professor. He has since authored or coauthored numerous journal and conference articles. He has been engaged in research in the area of wireless communications and signal processing for 25 years both in academic and industrial organizations. His research interests include resource allocation in full duplex and cognitive dense networks, visual data communications over the IoT, applications in healthcare, and communication protocols for autonomous vehicle/drone networks. He is a fellow of the IET and Founder and Chair of the Wireless Advanced (formerly SPWC) annual International Conference from 2003 to 2018.

Jiancao Hou (S'09-M'15) received the B.S. degree in honor program (information science) from China Agricultural University, Beijing, China, in 2008, the M.Sc. degree with distinction in radio frequency communication systems from the University of Southampton, Southampton, U.K., in 2009, and the Ph.D. degree in electrical engineering from the University of Surrey, Guildford, U.K. in 2014. From 2014 to 2016, he was a research fellow with the Institute for Communication Systems (ICS), University of Surrey, Guildford, U.K.. Since 2017, he has been a research associate with the Centre for Telecommunication Research (CTR), King's College London, London, U.K., and strongly involved in the EPSRC SENSE project. His current research interests include interference cancellation for full-duplex dense networks, stochastic geometry theory, and MIMO beamforming techniques.

Mark F. Flanagan ((M'03-–SM'10) received the B.E. and Ph.D. degrees in electronic engineering from University College Dublin, Dublin, Ireland, in 1998 and 2005, respectively.

During 1998—1999, he was a Project Engineer with Parthus Technologies Ltd. Between 2006 and 2008, he held postdoctoral research fellowships with the University of Zurich, Switzerland; the University of Bologna, Italy; and the University of Edinburgh, U.K. In 2008, he was appointed as an SFI Stokes Lecturer in electronic engineering with University College Dublin, where he is currently an Associate Professor. In the summer of 2014, he was a Visiting Senior Scientist with the Institute of Communications and Navigation of the German Aerospace Center, under a DLR-DAAD fellowship. His research interests include information theory, wireless communications, and signal processing.

Dr. Flanagan is currently serving as a Senior Editor for IEEE COMMUNICATIONS LETTERS. He has served on the Technical Program Committees of several IEEE international conferences. He is a Senior Member of the IEEE (Communications and Signal Processing Societies).